Remote Sensing of Environment 112 (2008) 4318–4332

Contents lists available at ScienceDirect

Remote Sensing of Environment

journal homepage: www.elsevier.com/locate/rse

Generating vegetation leaf area index Earth system data record from multiple sensors. Part 2: Implementation, analysis and validation

Sangram Ganguly [a,*], Arindam Samanta [a], Mitchell A. Schull [a], Nikolay V. Shabanov [b], Cristina Milesi [c], Ramakrishna R. Nemani [c], Yuri Knyazikhin [a], Ranga B. Myneni [a]

[a] Department of Geography and Environment, Boston University, 675 Commonwealth Avenue, Boston, MA 02215, USA
[b] NOAA/NESDIS, 5200 Auth Rd., Camp Springs, MD 20746, USA
[c] Ecosystem Science and Technology Branch, NASA Ames Research Center, Mail Stop 242-4, Mofett Field, CA 94035, USA

ARTICLE INFO

Article history:
Received 28 February 2008
Received in revised form 28 July 2008
Accepted 29 July 2008

Keywords:
Leaf area index
Validation
Accuracy
Climate data
Long term data record
AVHRR LAI
MODIS LAI
CYCLOPES
Spectral invariants
Recollision probability
Radiative transfer
Scaling
Single scattering albedo
Data uncertainties

ABSTRACT

The evaluation of a new global monthly leaf area index (LAI) data set for the period July 1981 to December 2006 derived from AVHRR Normalized Difference Vegetation Index (NDVI) data is described. The physically based algorithm is detailed in the first of the two part series. Here, the implementation, production and evaluation of the data set are described. The data set is evaluated both by direct comparisons to ground data and indirectly through inter-comparisons with similar data sets. This indirect validation showed satisfactory agreement with existing LAI products, importantly MODIS, at a range of spatial scales, and significant correlations with key climate variables in areas where temperature and precipitation limit plant growth. The data set successfully reproduced well-documented spatio-temporal trends and inter-annual variations in vegetation activity in the northern latitudes and semi-arid tropics. Comparison with plot scale field measurements over homogeneous vegetation patches indicated a 7% underestimation when all major vegetation types are taken into account. The error in mean values obtained from distributions of AVHRR LAI and high-resolution field LAI maps for different biomes is within 0.5 LAI for six out of the ten selected sites. These validation exercises though limited by the amount of field data, and thus less than comprehensive, indicated satisfactory agreement between the LAI product and field measurements. Overall, the inter-comparison with short-term LAI data sets, evaluation of long term trends with known variations in climate variables, and validation with field measurements together build confidence in the utility of this new 26 year LAI record for long term vegetation monitoring and modeling studies.

© 2008 Elsevier Inc. All rights reserved.

1. Introduction

Long term global vegetation monitoring requires temporally and spatially consistent data sets of vegetation biophysical variables characteristic of vegetation structure and functioning like the Leaf area index (LAI) and Fraction of Photosynthetically Active Radiation (FPAR). Such data sets are useful in many applications ranging from ecosystem monitoring to modeling of the exchange of energy, mass (e.g. water and CO_2), and momentum between the Earth's surface and atmosphere (Demarty et al., 2007; Dickinson et al., 1986; Sellers et al., 1996; Tian et al., 2004). A key step in assembling these long term data sets is establishing a link between data from earlier sensors (e.g. AVHRR) and present/future sensors (e.g. MODIS TERRA, NPOESS) such that the derived products are independent of sensor characteristics and represent the reality on the ground both in absolute values and variations in time and space (Van Leeuwen et al., 2006). Multi-decadal globally validated data sets of LAI and FPAR produced with a physically based algorithm and of known accuracy are currently not available, although several recent attempts have resulted in shorter term data sets from medium resolution sensor data (Knyazikhin et al., 1998; Gobron et al., 1999; Chen et al., 2002; Yang et al., 2006a; Plummer et al., 2006; Baret et al., 2007). The typical target accuracy required for LAI is approximately 0.5 according to the Global Climate Observation System (GCOS, 2006). The MODIS stage 1 land validation efforts for the LAI/FPAR product based on field measurements show that MODIS LAI is an overestimate by about 12% (RMSE = 0.66) (WWW1; Yang et al., 2006a). The accuracy in the long term AVHRR LAI product is based on the MODIS LAI's definition of accuracy as MODIS LAI serves as the benchmark for our analysis.

In the first of this two paper series (Ganguly et al., in press), we presented a physically based approach for deriving LAI and FPAR products from AVHRR data that are of comparable quality to the MODIS products. The approach is based on the radiative transfer theory of canopy spectral invariants which facilitates parameterization of the canopy spectral bidirectional reflectance factor

DOI of original article: doi:10.1016/j.rse.2008.07.014.
* Corresponding author. Tel.: +1 617 353 8846; fax: +1 617 353 8399.
E-mail address: sganguly@bu.edu (S. Ganguly).

0034-4257/$ – see front matter © 2008 Elsevier Inc. All rights reserved.
doi:10.1016/j.rse.2008.07.013

(BRF). The methodology permits decoupling of the structural and radiometric components and is applicable to any optical sensor. However, it requires a set of sensor-specific values of configurable parameters, namely the single scattering albedo and data uncertainty, in order to maintain consistency in the derived products.

In this second paper, we present an evaluation of a new global monthly LAI data set derived from the AVHRR NDVI for the period July 1981 to December 2006 with the algorithm presented in the first paper. The outline of this paper is as follows. The implementation of the algorithm and production of the data set are first detailed. The data set was evaluated both by direct comparisons to ground data and indirectly through inter-comparisons with similar data sets. This indirect validation included comparisons with MODIS and CYCLOPES LAI products at a range of spatial scales, and correlations with key climate variables in areas where temperature and precipitation limit plant growth. The data set was also analyzed to examine spatio-temporal trends and inter-annual variations in vegetation activity that have been reported previously in the literature. Direct validation included comparisons to field data from several campaigns conducted as part of the Land Product Validation Subgroup (LPV) of the Committee Earth Observing Satellite (CEOS) (Justice et al., 2000; Morisette et al., 2006). In the final section, conclusions from the production and evaluation exercises are presented.

2. Production of the LAI dataset

This section provides a schematic of the algorithm implementation as well as a brief description of the input datasets and LAI retrieval mechanism. The MODIS Collection 5 (C5) LAI product over the period of overlap between the two sensors (2000 to 2002) is taken as a benchmark in this study. Descriptions related to satellite input data and land cover classification map are provided in Section 2.1. A step-by-step implementation of the theoretical framework (Ganguly et al., in press) is given in Sections 2.2 and 2.3. The LAI product is described in Section 2.4.

2.1. Input satellite data and land cover classification map

The 15-day maximum value AVHRR NDVI composites (Holben, 1986) from the NASA GIMMS group for the period July 1981 to December 2006 are used as the input data in this study (Tucker et al., 2005). The data are at 8 km spatial resolution in a geographic latitude–longitude projection and have been corrected for loss of calibration, view and solar zenith angle variations, contamination from volcanic aerosols, and other effects not related to vegetation change (Pinzon et al., 2005; Tucker et al., 2005). The maximum value compositing diminishes the atmospheric effects such as sensitivity of the AVHRR wide spectral bands to the presence of water vapor, ozone, etc (Brown et al., 2006) minimizing residual atmospheric and cloud contamination (Holben, 1986). The average of the two 15-day maximum value composites was used to generate the monthly 8 km LAI product.

The latest version (C5) of the MODIS LAI data set was used as a benchmark in the production of the AVHRR LAI data set (Shabanov et al., 2005; Yang et al., 2006b). The monthly 1 km MODIS data set was aggregated to 8 km spatial resolution. In the aggregation process, the LAI value of the 8 km pixel is calculated as the mean over 1 km LAI values of high quality only. The high quality retrievals refer to LAI values generated by the C5 MODIS LAI/FPAR algorithm (Yang et al., 2006b). Further, the quality flag value for the 8 km pixel is evaluated as the percentage of the corresponding sixty four 1 km pixels of high quality. This 8 km MODIS data set was then re-projected to the geographic latitude–longitude projection from its native ISIN projection. For the inter-comparison of AVHRR and MODIS LAI (Section 3), only 8 km MODIS LAI pixels with quality flag values greater than 90% were used (WWW2, Yang et al., 2006b). Similarly, only main RT algorithm AVHRR retrievals (Section 2.3) were used when inter-comparing the data sets.

The land cover map (or biome classification map) is a key ancillary input to the LAI retrieval process. The C5 MODIS LAI/FPAR operational algorithm references a 1 km eight biome classification map consisting of the following classes: (1) grasses and cereal crops, (2) shrubs, (3) broadleaf crops, (4) savannah, (5) evergreen broadleaf forests, (6) deciduous broadleaf forests, (7) evergreen needleleaf forests, (8) deciduous needleleaf forests (Yang et al., 2006a). We used the same map but at 8 km resolution by retaining the most frequently occurring land cover amongst the sixty four 1 km pixels (Tian et al., 2002).

2.2. Achieving consistency with the Terra MODIS LAI products

The AVHRR mode of the proposed algorithm accepts inputs of surface reflectances as projections of the simple ratio (SM = near-infrared / red reflectances) line onto the red-NIR spectral axes, i.e., the red and NIR reflectance are proportional to cos α and sin α, respectively, where $\alpha = \tan^{-1}(\mathrm{NIR}/\mathrm{RED}) = \tan^{-1}(\mathrm{SM})$ (Ganguly et al., in press). Errors in cos α and sin α are determined by errors in the NDVI data. The consistency conditions of the multi-sensor LAI algorithm (Ganguly et al., in press) are:

(a) The algorithm should generate a set of acceptable solutions given AVHRR NDVI;
(b) This set should include all acceptable solutions generated by the MODIS algorithm when given the corresponding AVHRR spectral reflectances;
(c) The algorithm should also be capable of admitting AVHRR spectral reflectances, in addition to NDVI, and generate the same set of acceptable solutions as the MODIS algorithm.

These conditions ensure that the difference between mean LAI values from the AVHRR (using NDVI as input) and MODIS (using spectral reflectance as input) modes of the algorithm is minimized. Specifically, the adjustment procedure was reduced to finding values of sensor-specific input plus model uncertainty and single scattering albedo for which

a) The consistency conditions are met;
b) The retrieval index (RI) is maximized;
c) The difference (RMSE) between AVHRR and MODIS LAI is minimized.

The retrieval index is the ratio of the number of pixels for which the algorithm retrieves a value of LAI to the total number of processed pixels,

$$\mathrm{RI} = \frac{\text{number of retrieved pixels}}{\text{total number of processed pixels}}. \tag{1}$$

The RI is a function of uncertainties in modeled and observed reflectances (or, the simple ratio) and the total number of spectral bands used. In general, the RI increases with increasing values of uncertainties (Fig. 1a and b) but at the same time, higher values of uncertainty refer to poor quality input data, and thus, poor quality retrievals.

The RMSE is defined as the root mean square error between the output AVHRR LAI image and the corresponding MODIS LAI image,

$$\mathrm{RMSE}(\varepsilon, \boldsymbol{\omega}) = \sqrt{\frac{1}{N}\sum_{k=1}^{N}\left[\mathrm{LAI}_{\mathrm{AVHRR}}(\varepsilon, \boldsymbol{\omega}; k) - \mathrm{LAI}_{\mathrm{MODIS}}(k)\right]^2}. \tag{2}$$

Here $\mathrm{LAI}_{\mathrm{AVHRR}}$ represents LAI values generated by the AVHRR mode of the algorithm given the relative uncertainty ε and the single scattering albedo $\boldsymbol{\omega}$, and $\mathrm{LAI}_{\mathrm{MODIS}}$ denotes the aggregated MODIS LAI values. The summation is performed over all 8 km vegetated pixels in a given image. The RMSE is a function of the relative uncertainty, single scattering albedo, landcover type and the image size. The following procedure was implemented to achieve efficient production of AVHRR LAI on a global scale.

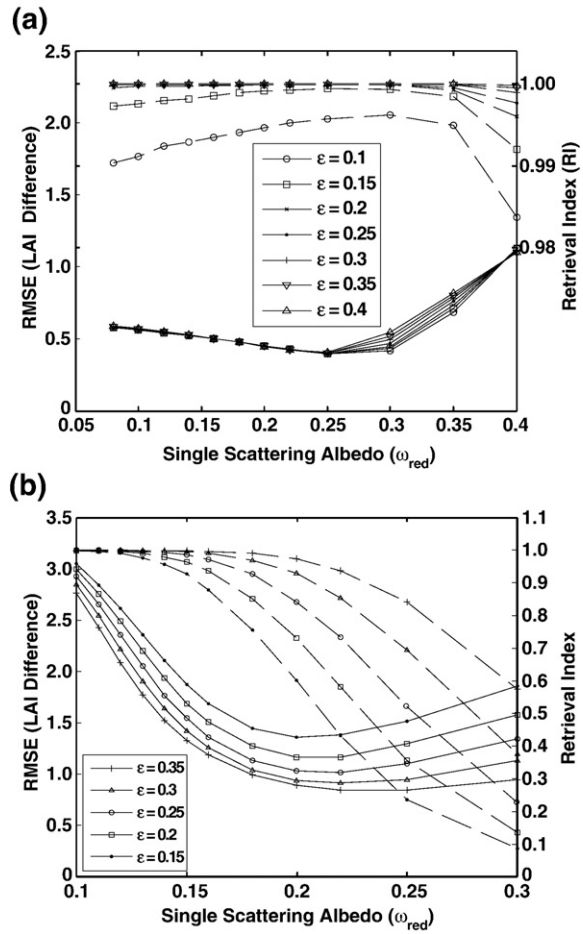

Fig. 1. The difference (RMSE) between MODIS and AVHRR LAI values (vertical axis on the left side and solid lines) and the Retrieval Index (vertical axis on the right side and dashed lines) as a function of the relative uncertainty $\varepsilon = \sigma_{RED}/RED$ and single scattering albedo at red spectral band. Optimal values of the single scattering albedo and the uncertainty should minimize RMSE and maximize the retrieval index. Simultaneously available AVHRR NDVI and MODIS C5 LAI data sets over grasses and cereal crops (panel (a), MODIS tile h10v05) and broadleaf deciduous forests (panel (b), MODIS tile h12v04) for the year 2001 are used in this example.

The configurable parameters, relative uncertainty (ε) and single scattering albedo (ω) at the red, are varied to minimize RMSE and maximize RI. Since uncertainties in the NIR reflectance are minimally impacted by the differences in spectral bandwidth and data resolution (Miura et al., 2000; Van Leeuwen et al., 2006; Section 5 in Ganguly et al., in press), their values are taken from the corresponding MODIS LUT and kept constant in the tuning procedure. This process is illustrated in Fig. 1. The RI increases with increasing values of ε_{RED}. A value of ε_{RED} of 30% generally yields a RI value of 90% or more for single scattering albedo at the red spectral band of less than ~0.2. ε_{RED} values greater than 30% are usually not considered as they represent poor quality input data (Fig. 3a and b in Tan et al., 2005a,b) and thus unreliable LAI retrievals. Also, for a preset value of ε_{RED}, the RMSE is minimum for a specific value of ω_{red} (ω_{red}=0.25 in Fig. 1a and ω_{red}=0.22 in Fig. 1b). Thus, for each vegetation type, an AVHRR LUT can be created consisting of the spectral BRF values calculated with optimum values of the single scattering albedo. Optimal values of the relative uncertainties are then used to specify the merit function (see Eq. (11) in Ganguly et al., in press).

We performed extensive analyses of the above procedure for all months of the year 2001, biome-by-biome, in order to examine variations in the configurable parameters with biome type and month (Table A1, Appendix A). We found that their optimal values exhibit a non-negligible variation with respect to the biome type and a weak sensitivity to the month. For each biome type, mean values over months are taken as instrument specific configurable parameters and used to generate global AVHRR LAI time series.

2.3. Global LAI production

Consider an input pixel from the AVHRR NDVI map representing a certain vegetation class. The algorithm queries the corresponding AVHRR LUT for this class and calculates the mean value and standard deviation (dispersion) of LAI from the retrieved solution set (Ganguly et al., in press). A successful retrieval is classified as a main algorithm retrieval. If the retrieval is unsuccessful, a backup algorithm similar to the MODIS approach is adopted, where the input simple ratio will be used to calculate a LAI value based on NDVI–LAI empirical relations (Yang et al., 2006a). An additional land cover quality control flag is incorporated which reports the percentage of the modal land cover type used in the retrieval of each 8 km AVHRR LAI pixel. A schematic representation of the algorithm implementation is shown in Fig. 2.

2.4. LAI data dissemination

The data set is stored as monthly LAI values together with their standard deviation and quality control flags at 8 km resolution in a geographic latitude–longitude projection for the period July 1981 to December 2006. The accuracy of the AVHRR LAI product is comparable to the MODIS LAI (cf. later sections), but with increased dispersion, which reflects the lower information content of AVHRR input (NDVI) compared to the MODIS input (spectral reflectances).

3. Results: comparison with other satellite LAI products

3.1. Assessment of AVHRR LAI for the tuning year

We performed a global scale assessment of the AVHRR LAI data set for the overlapping year 2001 for which MODIS LAI was used as a

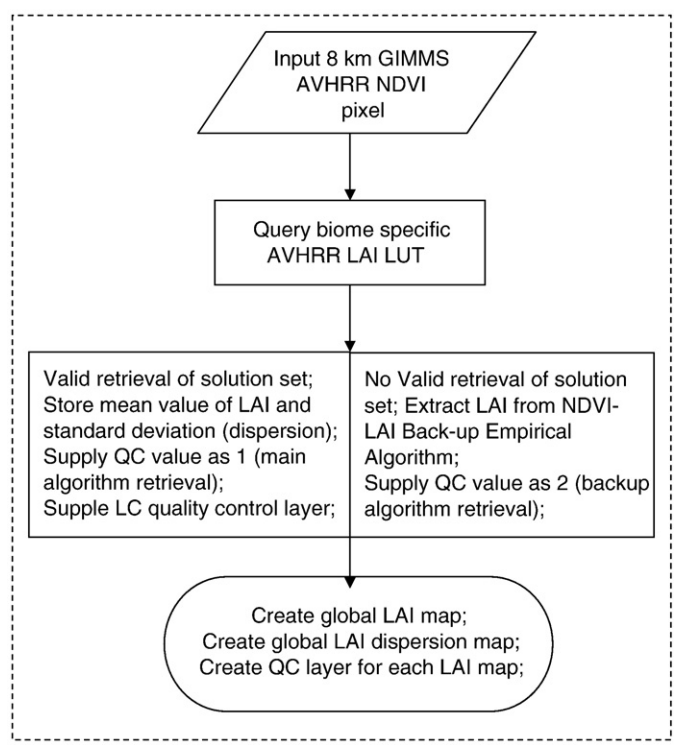

Fig. 2. Flowchart showing global LAI production.

Table 1
Global scale analysis of LAI differences across different biomes for different months and for annual maximum LAI

Month	Biome 1		Biome 2		Biome 3		Biome 4		Biome 5		Biome6		Biome 7		Biome 8	
	$\bar{\delta}$	σ	$\bar{\delta}$	σ	$\bar{\delta}$	σ	$\bar{\delta}$	σ	$\bar{\delta}$	σ	$\bar{\delta}$	σ	$\bar{\delta}$	σ	$\bar{\delta}$	σ
January	0.0393	0.358	0.0139	0.176	0.062	0.50	−0.050	0.922	−0.004	1.798	0.167	0.603	0.036	0.772	0.009	0.107
April	−0.069	0.360	0.026	0.246	0.0001	0.479	−0.081	1.049	−0.341	1.879	−0.169	0.619	−0.358	0.457	−0.319	0.162
July	0.145	0.948	0.253	0.942	−0.065	0.813	−0.078	0.942	0.150	1.780	0.421	1.528	−0.236	1.116	−0.147	1.175
October	0.028	0.414	−0.045	0.216	0.076	0.639	−0.012	0.967	−0.018	1.70	0.007	0.683	−0.242	0.474	−0.018	0.176
Peak LAI	0.367	1.207	0.292	1.024	0.402	1.246	0.560	1.399	0.325	1.103	0.610	1.313	−0.202	1.154	−0.146	1.206

$\bar{\delta}$=mean value of the LAI difference (accuracy). LAI difference is defined as (AVHRR LAI−MODIS LAI).
σ=standard deviation (precision) of the LAI difference.

reference for tuning the AVHRR algorithm. The quality of the AVHRR product depends on the quality of input NDVI and land cover data. The input land cover map is the same for both MODIS and AVHRR, therefore the input AVHRR NDVI and/or MODIS reflectance data determine the quality of retrieved LAI. A pixel data is considered reliable only if the MODIS quality flag for the corresponding pixel corresponds to a best quality retrieval and simultaneously has an AVHRR RT algorithm retrieval. For each biome, all such pixels are selected for analysis over the course of a year. A month by month spatial difference, defined as delta LAI (δ_{LAI}) for each such pixel over a particular biome type is calculated as

$$\delta_{LAI}(i_b, j_b, t) = \mathrm{AVHRR}_{LAI}(i_b, j_b, t) - \mathrm{MODIS}_{LAI}(i_b, j_b, t). \quad (3)$$

Here i_b, j_b are pixel coordinates for a specific biome "b" and "t" is the month. Table 1 shows the accuracy ($\bar{\delta}$=mean value of δ_{LAI} (i_b, j_b, t)) and precision (σ=standard deviation of δ_{LAI} (i_b, j_b, t)) of AVHRR LAI with respect to MODIS LAI for different biomes and four different months. The last row in Table 1 shows $\bar{\delta}$ calculated from annual maximum LAI values, which reflect the worst possible case.

The herbaceous biomes (grasses/cereal crops, shrubs, broadleaf crops, savannas) show a $|\bar{\delta}|$ in the range of zero to 0.25 LAI in all the four months, while the woody biomes (broadleaf and needleleaf forests) show a $|\bar{\delta}|$ from nearly zero to 0.42 LAI. AVHRR LAI underestimates MODIS LAI especially in the savannas and needleleaf forests. The accuracy of annual maximum LAI is usually within ±0.6 LAI for most of the vegetation classes. The precision is always within ±0.65 standard deviation units. In deciduous broadleaf forests, peak annual AVHRR LAI overestimates its MODIS equivalent by almost 0.61 LAI. This is due to uncertainty in input NDVI and differences in the time of the year at which the peak LAI value exists in these products. These larger differences suggest that LAI retrievals from NDVI (low information content) will poorly capture the seasonality in comparison to LAI retrievals from surface reflectances (higher information content). The input information content and uncertainties control whether the retrievals are over- or underestimates, which in our case is not systematic as shown in Fig. 3 and Table A2 in Appendix A. Pixels with greater than ±0.6 LAI difference constitute only 3.3% of the total global vegetated pixels. Overall, the difference values indicate spatio-temporal agreement between the AVHRR and MODIS LAI data sets as well as acceptable levels of accuracy (within 0.5 LAI) and precision, suggesting that the tuning process has been successfully implemented.

3.2. Comparison with MODIS C5 LAI data

The inter-comparison of AVHRR and MODIS data sets for a three year period (2000 to 2002) is presented here. The choice of these years is dictated by the availability of latest version of MODIS products (C5).

3.2.1. Global scale inter-comparison

Fig. 4a shows a comparison between the mean monthly AVHRR and MODIS LAI for each of the 8 vegetation classes. The AVHRR values explain 97.5% of the variability in MODIS values and on average will be in error in their estimation by 0.18 LAI. This comparison indicates qualitative agreement between the two data sets; however, global averaging over all pixels of a particular vegetation class masks the underlying variability in LAI amongst those pixels. Therefore, an inter-comparison at regional and local scales was performed, as reported below.

3.2.2. Regional scale inter-comparison

Grasslands and evergreen needleleaf forests were considered for a regional scale inter-comparison exercise. Mean seasonal values – DJF (December to February), MAM (March to May), JJA (June to August), and SON (September to November) – for a homogeneous region of 100

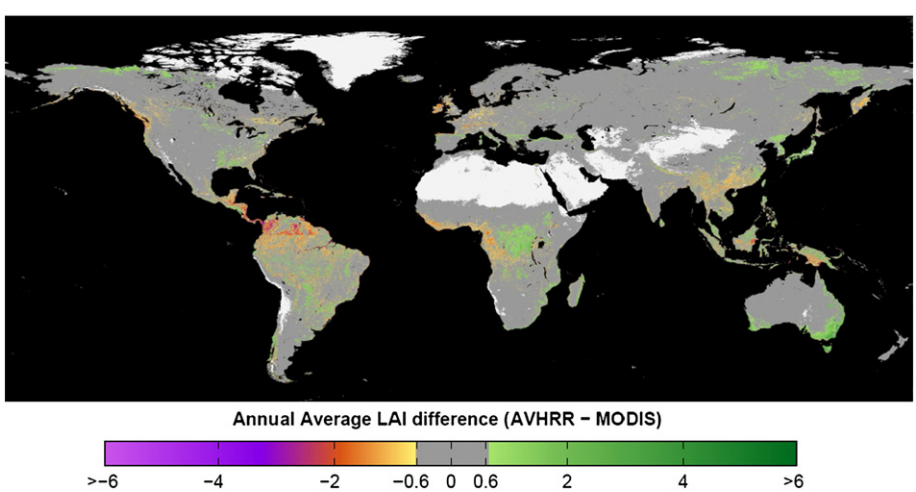

Fig. 3. Average annual LAI difference (AVHRR minus MODIS) for the year 2001. The grey areas represent changes within ±0.6 LAI units (96.7% of the total vegetated pixels). Areas with black color represent water bodies and white color denotes non-vegetated pixels or snow. Land pixels with LAI differences greater than ±0.6 represent only 3.3% of the total vegetated pixels globally.

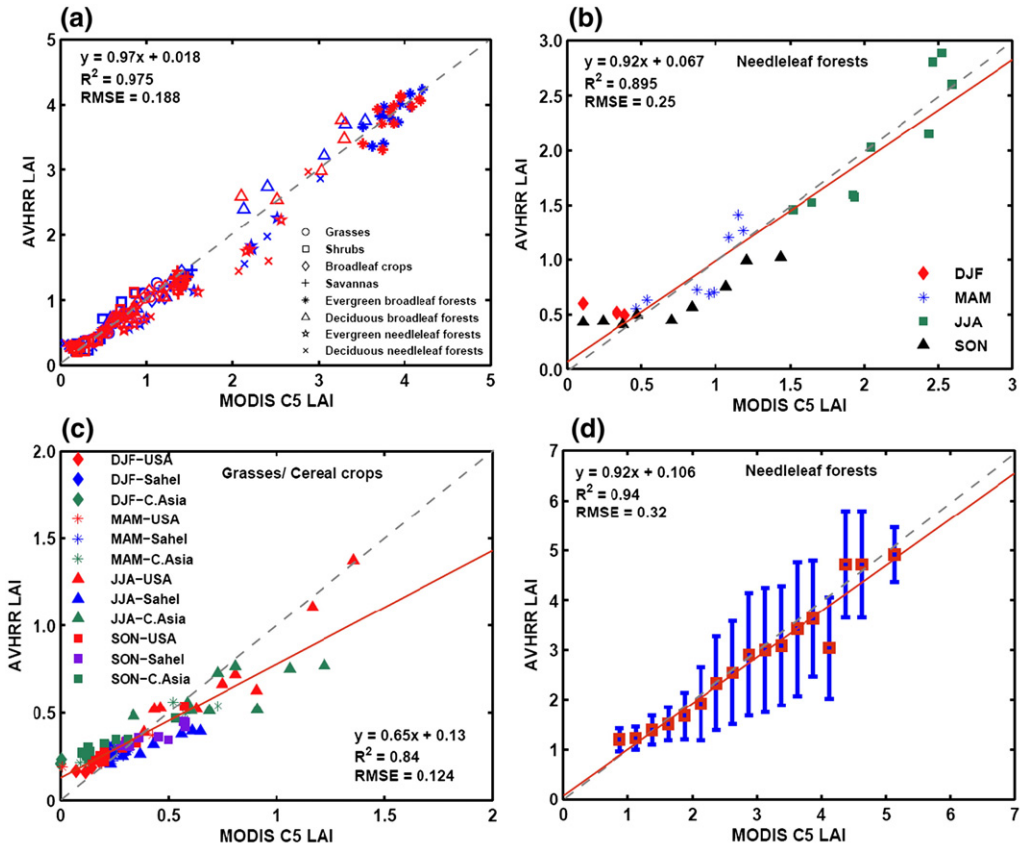

Fig. 4. Panel (a) shows comparison between MODIS and AVHRR LAI for the year 2001 (blue color) and 2002 (red color) for different vegetation classes. The LAI values are globally averaged values for the respective vegetation pixels. A similar comparison between MODIS and AVHRR LAI for years 2000–2002 but for different seasons on homogeneous patches of evergreen needleleaf forests in Western Russia (Panel b) and grasslands in the USA, Sahel and Central Asia (Panel c). Panel (d) shows a comparison between MODIS and AVHRR LAI values averaged from June to August, 2001, over a homogeneous patch of evergreen needleleaf forests in Western Russia. For each MODIS LAI bin, the corresponding AVHRR LAI values were averaged (red box) to reduce scatter. The error bars represent the dispersion of the AVHRR LAI values within each bin. (For interpretation of the references to color in this figure legend, the reader is referred to the web version of this article.)

by 100 evergreen needleleaf forest pixels in Western Russia were calculated for the period 2000 to 2002 and shown in Fig. 4b. The R^2 (0.895) and RMSE (0.25) indicate good agreement between the two data sets. The dispersion does not exceed 0.5 LAI. Fig. 4c is a similar plot for three homogeneous grassland sites, 100×100 pixels each, located in the Great Plains of the USA, the Sahel and Central Asia. Again, the R^2 (0.84) and RMSE (0.12) indicate a satisfactory agreement between the two data sets. Some scatter at LAI values greater than 1.25 is seen which is within the accuracy limit of 0.5 LAI (GCOS, 2006).

3.2.3. Local scale inter-comparison

The June to August mean LAI of a homogeneous patch of 50 by 50 evergreen needleleaf forest pixels in western Russia was used for local scale inter-comparison between the two data sets. Fig. 4d shows the mean and dispersion of AVHRR LAI as a function of MODIS LAI. The regression relation in Fig. 4d has R^2 of 0.94 and RMSE of 0.32 which indicate overall correspondence between the two data sets, although some dispersion can be seen at LAI values greater than 3.

3.3. Comparison with CYCLOPES LAI product

The Carbon Cycle and Change in Land Observational Products from an Ensemble of Satellites (CYCLOPES) LAI product (version 3.1) was derived from data from the SPOT/VEGETATION sensor over a 1/112° plate-carrée spatial grid and 10-day frequency (Baret et al., 2007). This product has reached a reasonable level of maturity as compared to MODIS LAI and shows satisfactory agreement with field measured values of LAI (Weiss et al., 2007). CYLOPES products from a select Benchmark Land Multisite Analysis and Intercomparison of Products (BELMANIP) benchmark network of sites (Baret et al., 2006) are utilized here (Table A3, Appendix A). The land surface type of each BELMANIP site is defined using the ECOCLIMAP (a global database of land surface parameters at 1 km resolution in meteorological and climate models) classification (Masson et al., 2003), which classifies the land into seven main categories. This inter-comparison was done for four vegetation types — needleleaf forests, grasslands, savannas and croplands. For each vegetation type, we chose representative sites (each site with a dominant biome type), each 50×50 km^2 (about 7×7 AVHRR pixels) in area, and calculated the mean monthly LAI values for the period 2001 to 2003 using simultaneously available AVHRR and CYCLOPES pixels that cover the same areas (Fig. 5). Mean values accumulated over areas composed of 20 or more AVHRR pixels were used in our inter-comparison analyses.

In grasslands and needleleaf forests, the AVHRR and CYCLOPES LAI values are close to the 1:1 line — slopes are 0.85 and 0.88, respectively and corresponding offsets are 0.17 and −0.05 (Fig. 5a and b). They explain 80% and 68% of the variability in CYCLOPES LAI and will be in error by 0.32 and 0.47 LAI on average. The correlation between the two products in the case of croplands is R^2=0.77 and for savannas, R^2=0.85; they differ by 0.34 LAI (croplands) and 0.24 LAI (savannas) (Fig. 5c and d). The deviation of AVHRR-CYCLOPES relationships from the 1:1 line is larger compared to grasslands and needleleaf forests (Fig. 5a and b). The deviations can partly be explained by the narrow dynamic range of LAI values, which is comparable to variation due to observation errors (Huang et al., 2006; Tan et al., 2005a,b; Wang et al., 2001). In this example, mean (standard deviation) values of CYCLOPES LAI over croplands and savannas are 0.87 (0.5) and 0.52 (0.5), respectively. Corresponding values of the AVHRR LAI are 0.73 (0.2)

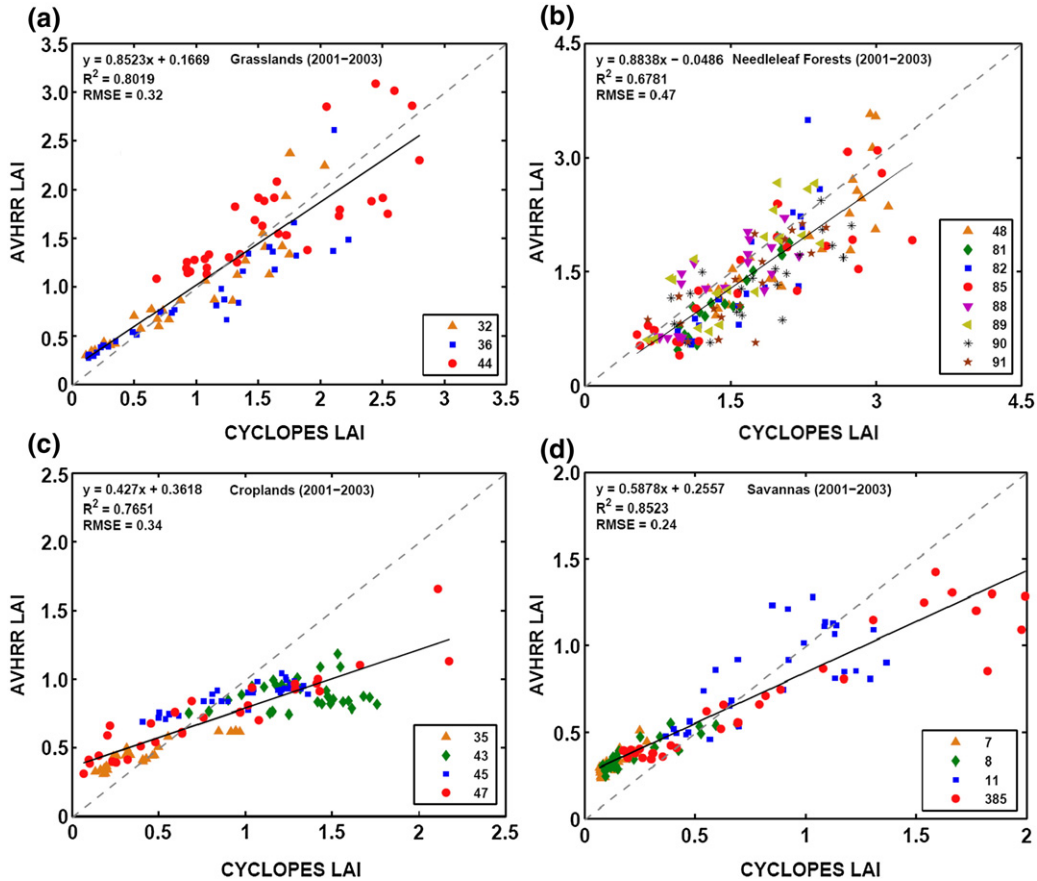

Fig. 5. Panels (a) to (d) show comparison between CYCLOPES and AVHRR LAI values for years 2001 to 2003 and different vegetation classes over the BELMANIP site database. The site numbers in the legend are given in Table A3 of Appendix A.

and 0.56 (0.32). Although there is variation in the comparability between the two data sets not only across vegetation types but also across sites with in a vegetation class, the disagreement does not exceed the disagreement between AVHHR LAI and ground truth data (Section 5).

4. Comparison with climate variables

In the absence of long term field LAI measurements spanning a couple of decades, another way to evaluate the data set is to compare temporal LAI trends with well-documented trends in vegetation growth and their relationship to temperature and precipitation anomalies in areas where these climatic variables limit plant growth (Buermann et al., 2003). The ability of the LAI data set to track vegetation changes due to surface temperature variations in the northern latitudes and precipitation changes in the semi-arid regions is evaluated in Sections 4.1 and 4.2. We isolate well correlated modes of co-variability between temperature, precipitation and LAI, and assess the relationship to large-scale circulation anomalies associated with the El Niño-Southern Oscillation (ENSO) and Arctic Oscillation (AO) in Section 4.3.

4.1. LAI variation with surface temperature in the northern latitudes

The northern latitudes, 40° to 70° N, have witnessed a persistent increase in growing season vegetation greenness related to unprecedented surface warming during the period 1981 to 1999 (Myneni et al., 1997; Slayback et al., 2003; Zhou et al., 2001). This greening was observed in Eurasia and less prominently in North America (Zhou et al., 2001). In fact, a decline in greenness was observed in parts of Alaska, boreal Canada and northeastern Eurasia (Barber et al., 2000; Goetz et al., 2005). The studies have used AVHRR NDVI data sets. Our slightly longer LAI data set facilitates a re-assessment of these changes. We calculated spatial trends (in %) in growing season, April to October, LAI for the region 40° to 70° N, for the periods 1982 to 1999 and 1982 to 2006. The greening trend (Fig. 6a) is evident in Eurasia, Northern Alaska, Canada and parts of North America, for the period 1982 to 1999. When this analysis is extended to 2006 (Fig. 6b), it is found that large contiguous areas in North America, Northern Eurasia and Southern Alaska show a decreasing trend in growing season LAI. This browning trend, especially in the boreal forests of Southern Alaska, Canada and in the interior forests of Russia have been reported in recent studies using AVHRR NDVI data (Angert et al., 2005; Goetz et al., 2005).

The spatial (40°–70° N) and growing season (April to October) averages of standardized anomalies (anomalies normalized by their standard deviation) of LAI, NDVI and surface temperature (Hansen et al., 1999) are shown in Fig. 7 for tundra and needleleaf forests, separately for North America and Eurasia. The anomaly of a given variable is defined as the difference between its growing season (April to October) mean in a given year and the growing season mean over the 1982 to 2006 time interval. The standardized anomalies of LAI and NDVI track each other very well (Table 2), that is, the long term trends in the LAI product are not an artifact of the LAI data set or the retrieval algorithm.

Our results indicate that vegetation activity significantly correlates with trends in surface temperature in the Eurasian and North American tundra over the entire period of the record (Table 2). This is consistent with reports of persistent greening in the tundra and evidence of shrub expansion in northern Alaska and the pan-Arctic (Goetz et al., 2005; Tape et al., 2006).

A decreasing trend in vegetation greenness is observed after 1996–97 period despite a continuing warming trend in the North American needleleaf forests. The regression model of LAI vs. surface temperature and time is statistically significant at the 10% level for the period 1982

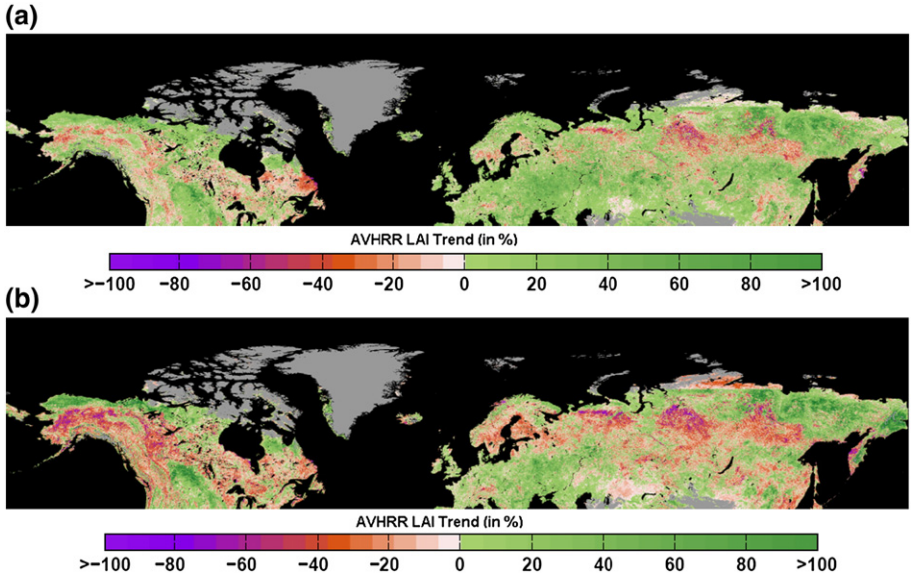

Fig. 6. Trends in AVHRR LAI for the growing season, April to October, for the region 40° N to 70° N, for the periods 1982 to 1999 (panel (a)) and 1982 to 2006 (panel (b)). For each 8 km AVHRR LAI pixel, the April to October mean LAI was regressed on time (years). The slope obtained from this regression, which if statistically significant based on the *t* statistic at or lower than 10% level, was converted to a percent trend by multiplying by the number of years times 100 and dividing by the mean April to October AVHRR LAI of 1982.

to 1999 but is statistically insignificant for the period 1982 to 2006 (Table 2). Similar patterns are observed in the Eurasian needleleaf forests also. These results imply a decreasing trend in vegetation activity possibly due to warming induced drought stress as has been suggested previously (Barber et al., 2000; Bunn & Goetz, 2006; Lapenis et al., 2005; Wilmking et al., 2004). There also have been reports of declining growth and health of white spruce trees in Alaska, enhanced insect disturbance in southern Alaska, and increase in fire frequency and severity in Alaska, Canada and Siberia during the past 6 to 7 years of consistent warming (Soja et al., 2007). These changes buttress the need for continued monitoring of vegetation activity in these northerly regions in the face of unprecedented climatic changes.

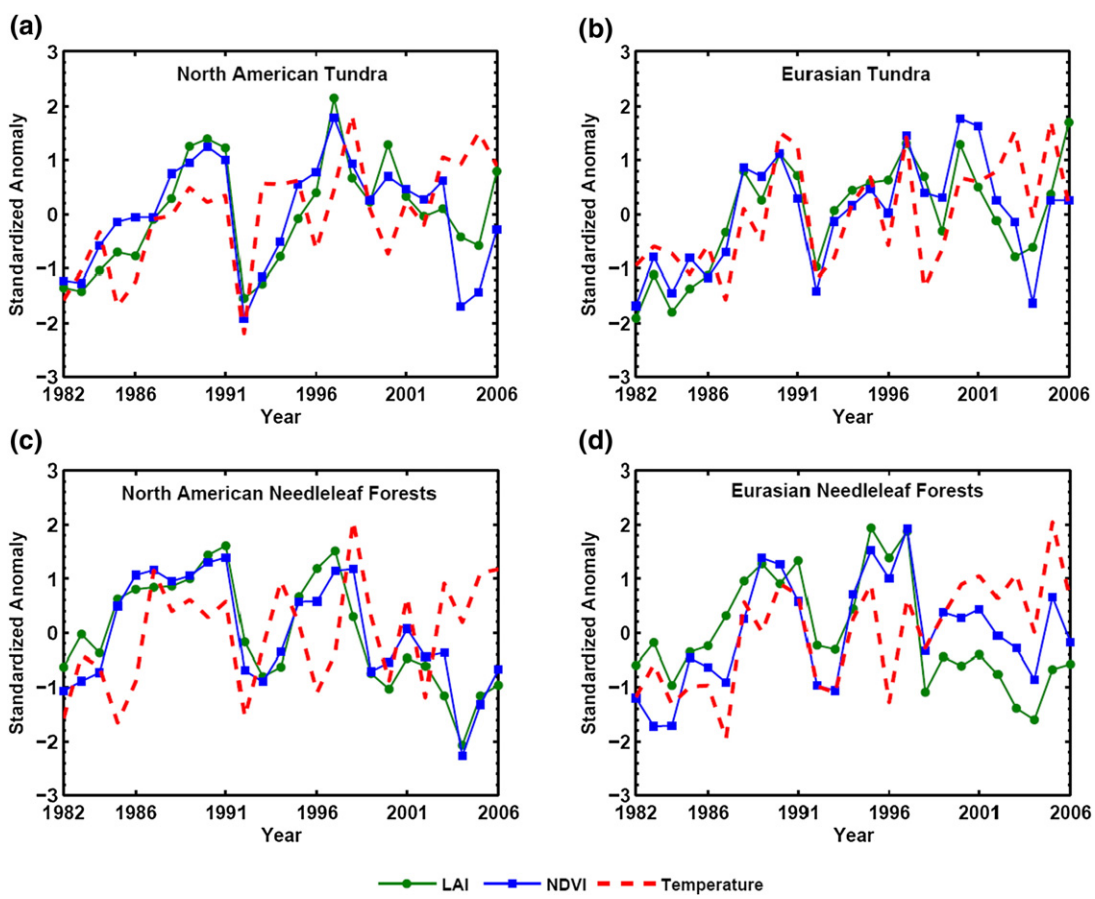

Fig. 7. Standardized April to October anomalies of AVHRR LAI (green), AVHRR NDVI (blue), and GISS Temperature (red dashed line) for Eurasian and North American needleleaf forests (panels (c) and (d)) and tundra (panels (a) and (b)) from 1982 to 2006. (For interpretation of the references to color in this figure legend, the reader is referred to the web version of this article.)

Table 2
Relationship between LAI, NDVI and Temperature anomalies in Eurasia (EA) and North America (NA) during the time period 1982 to 2006 and 1982 to 1999

	$LAI=\beta_o+\beta_1 \cdot Temp+\beta_2 \cdot t+\varepsilon$			$\Delta LAI=\beta_o+\beta_1 \cdot \Delta Temp+\varepsilon$			$NDVI=\beta_o+\beta_1 \cdot Temp+\beta_2 \cdot t+\varepsilon$			$\Delta NDVI=\beta_o+\beta_1 \cdot \Delta Temp+\varepsilon$		
	R^2	β_1	*t* staticstic	R^2	β_1	*t* staticstic	R^2	β_1	*t* staticstic	R^2	β_1	*t* staticstic
NA tundra	0.235	0.02	1.41[c]	0.07	0.012	1.28[c]	0.05	0.004	0.65[c]	0.07	0.005	(1.28)[c]
	(0.373)	(0.032)	(1.83)[b]	(0.2)	(0.021)	(1.80)[b]	(0.317)	(0.009)	(1.67)[c]	(0.27)	(0.007)	(1.79)[b]
NA	0.29	0.03	(0.92)[d]	0.01	0.011	0.5[d]	0.20	0.01	1.52[c]	0.14	0.007	(1.89)[c]
Needleleaf forest	(0.02)	(0.02)	(0.48)[c]	(0.008)	(0.030)	(0.10)[d]	(0.14)	(0.01)	(1.33)[c]	(0.1)	(0.006)	(1.31)[c]
NA (all biomes)	0.04	0.019	0.44[d]	0.009	0.007	0.46[d]	0.11	0.008	1.34[c]	0.157	0.007	(2.1)[b]
	(0.23)	(0.01)	(1.25)[b]	(0.006)	(0.006)	(1.13)[c]	(0.33)	(0.009)	(1.84)[b]	(0.181)	(0.007)	(1.82)[b]
EA tundra	0.42	0.028	1.73[b]	0.2	0.025	2.41[b]	0.05	0.006	1.02[c]	0.17	0.007	2.16[b]
	(0.75)	(0.042)	(3.73)[a]	(0.45)	(0.34)	(3.43)[a]	(0.40)	(0.007)	(1.82) [b]	(0.31)	(0.006)	(2.01) [b]
EA	0.18	0.09	1.70[c]	0.27	0.09	2.91[b]	0.26	0.01	2.48[b]	0.3	0.01	3.71[a]
Needleleaf forest	(0.43)	(0.13)	(2.29)[b]	(0.30)	(0.11)	(2.57)[b]	(0.6)	(0.017)	(2.94)[b]	(0.4)	(0.011)	(2.61)[b]
EA (all biomes)	0.12	0.06	1.46[c]	0.30	0.06	3.0[a]	0.11	0.009	1.546[c]	0.38	0.009	3.87[a]
	(0.63)	(0.082)	(2.53)[b]	(0.43)	(0.075)	(3.06)[a]	(0.7)	(0.012)	(3.10)[a]	(0.44)	(0.009)	(3.42)[a]

LAI and NDVI are April–October average values between 40° N and 70° N. Temp (temperature) is the near surface air temperature anomalies (base period 1951–1980) between 40° N and 70° N.
[a]Statistically significant at the 0.001 level.
[b]Statistically significant at the 0.05 level.
[c]Statistically significant at the 0.1 level.
[d]Statistically insignificant.
β_o and β_1 are regression coefficients and ε is the stochastic error term. LAI, NDVI, and Temp are all expressed as standardized anomalies. ΔLAI, ΔNDVI, and ΔTemp are the respective first differences.
The bracketed terms represent the regression statistics for the time period 1982–1999. The un-bracketed terms represent regression statistics for the period 1982–2006.

4.2. LAI variation with precipitation in the semi-arid tropics

The availability of water critically limits plant growth in the semi-arid tropical regions of the world, especially in grasslands where precipitation received in the wet months is the primary driver of plant growth (Hickler et al., 2005; Nemani et al., 2003; Prince et al., 2007). This relationship provides a basis for evaluating the LAI product by examining the correlation between LAI and precipitation variations (Huffman et al., 2007; Mitchell & Jones, 2005). We include NDVI in this analysis to argue that correlations observed between LAI and precipitation are not an artifact of the LAI algorithm if they are also seen in the NDVI data as well.

For the purposes of this analysis, we define semi-arid regions in the tropics and subtropics as those regions with peak annual NDVI values in the range 0.12 to 0.55. These regions approximately correspond to areas with annual total rainfall less than 700 mm. We selected four regions in the Eastern hemisphere for this study — Sahel, Southern Africa, Southeast Asia and Australia. The Sahelian region consisted of Senegal, Mauritania, Mali, Burkina Faso, Niger, Nigeria, Chad and Sudan; the Southern African region consisted of Botswana, South Africa and Namibia; and the Southeast Asian region spanning Afghanistan, Pakistan and India.

A highly significant correlation between variations in standardized anomalies of precipitation and annual peak vegetation greenness (LAI or NDVI) is seen in Australia, Sahel and Southern Africa (Fig. 8; Table 3). A slightly weaker correlation between these variables is observed in Southeast Asia. We also observed an increasing trend in precipitation and greenness in these semi-arid regions during the period of our study (1981 to 2006), in agreement with several recent reports on greening and increased precipitation in the Sahelian region (Herrmann et al., 2005; Hickler et al., 2005; Seaquist et al., 2006). The greenness increase in Southeast Asia (especially India) is not supported by enhanced precipitation and is therefore likely due to other factors such as irrigation and fertilizer use, but this needs to be further investigated. The strength of these correlations imbues confidence in the inter-annual variations embedded in the derived LAI product.

4.3. Canonical correlation analysis

The correlations observed between LAI and temperature in the northerly regions and between LAI and precipitation in the semi-arid areas raise a question about the mechanistic basis for these relations. It has been reported previously that large-scale circulation anomalies, such as the El Niño-Southern Oscillation (ENSO) and Arctic Oscillation (AO), explain similar correlations, but at the hemispheric scale (Buermann et al., 2003). The canonical correlation analysis (CCA) is ideally suited for this purpose as it seeks to estimate dominant and independent modes of co-variability between two sets of spatio-temporal variables (Barnett and Preisendorfer, 1987; Bjornsson and Venegas, 1997). The variables are linearly transformed into two new sets of uncorrelated variables called canonical variates, which explain the co-variability between the two original variables, in a descending order. Thus, most of the co-variability is captured by the first 2 to 3 canonical variates.

For the CCA in the North, each year is denoted as a variable (1982 to 2006, that is, 25 variables in total) and each pixel as an observation (the total number of observations is the number of vegetated pixels in the latitudinal zone 45° N and 65° N). The two sets of variables for CCA are the spring time (March to May) LAI and surface temperature anomalies at 1° resolution (Buermann et al., 2003). The anomalies were normalized by their respective standard deviation. The temperature and the LAI anomaly fields for each grid box were area-weighted with the square root of the respective grid box area to avoid geometrical effects (Buermann et al., 2002; North et al., 1992). Each of the set of 25 (time) variables was transformed to Principal Components (PCs) using singular value decomposition. In each case, only the first six PCs were retained as they explain a large fraction of the variance in the input set of variables. In the CCA, each canonical variate is a time series which accounts for a certain fraction of the co-variability between the variables (PCs). The first two canonical variates derived from each set of six PCs explained about 50% of the co-variability between the two sets of variables in our case.

We use the September to November (SON) NINO3 index (WWW3) to represent ENSO because the sea surface temperature anomalies then approach peak values during an ENSO cycle (Dai et al., 1997). Fig. 9a shows that the correlation between SON NINO3 index and first canonical variate related to LAI is very low ($r=0.1$). The same is true for the correlation between SON NINO3 index and the first canonical variate related to temperature anomalies. This is in contrast to a strong correlation reported in Buermann et al. (2003) for the period 1982 to 1998. This decline in correlation may be due to weak ENSO activity and/or changes in teleconnection patterns since the 1998–2000 period (WWW4). The correlation between the Arctic Oscillation (AO) index and the second canonical variates of both LAI

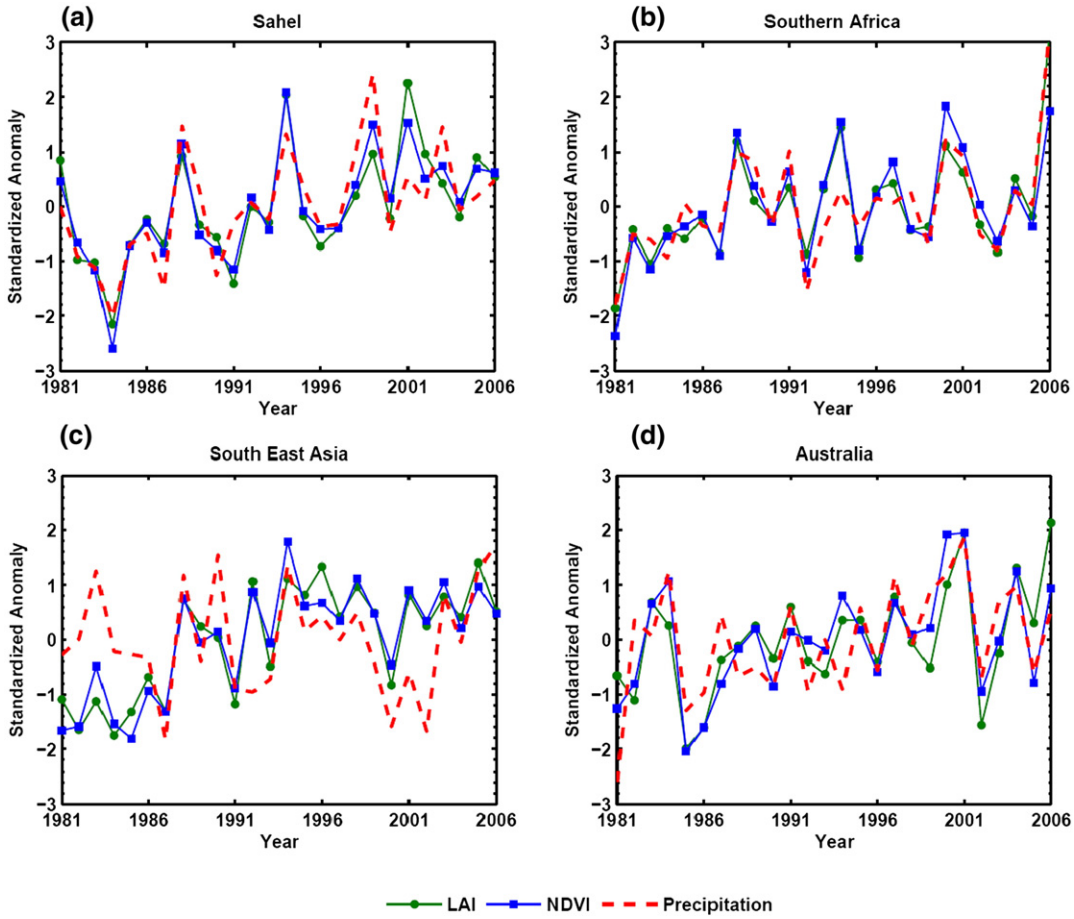

Fig. 8. Standardized anomalies of annual peak AVHRR LAI (green line), annual peak AVHRR NDVI (blue line) and annual peak (three wettest month CRU+TRMM) precipitation (red dashed line) for the semi-arid regions (panels (a)–(d)) from 1981 to 2006. (For interpretation of the references to color in this figure legend, the reader is referred to the web version of this article.)

and temperature is reasonably strong (0.45 and 0.61, respectively; Fig. 9b), consistent with the strong correlations reported by Buermann et al. (2003) for the period 1982 to 1998. Thus, the AO seems to continue to be a prominent driver of surface temperature (Thompson and Wallace, 1998) and plant growth variability in the northern latitudes.

We also performed CCA on standardized anomalies of annual maximum LAI and precipitation for the semi-arid regions of 40° N to 40° S latitudinal zone (cf. Section 4.2). The first two canonical variates explained about 50% of the co-variability between annual peak LAI and precipitation anomalies. A reasonable correlation is seen between the September to November NINO3 index and the first canonical variates of LAI and precipitation (0.33 and 0.32, respectively; Fig. 9c), consistent with several previous reports of ENSO influence on inter-annual variability in tropical and sub-tropical precipitation (Dai & Wigley, 2000; Ropelewski & Halpert, 1987). The correlation between the second canonical variates and the AO index is weak (Fig. 9d) which is not surprising as the AO is not known to be a driver of precipitation and thus plant growth variability in these regions.

In summary, the strong ENSO driven linked variations between northern vegetation greenness and surface temperature observed during the 1980s and 90s have weakened since 2000. The AO influence however continues to be strong. In the tropical and sub-tropical regions, the ENSO influence on linked variations between

Table 3
Relationship between annual maximum LAI, NDVI and three wettest month precipitation anomalies in the semi-arid tropics from 1981 to 2006

	$LAI=\beta_o+\beta_1 \cdot Prec+\varepsilon$			$\Delta LAI=\beta_o+\beta_1 \cdot \Delta Prec+\varepsilon$			$NDVI=\beta_o+\beta_1 \cdot Prec+\varepsilon$			$ANDVI=\beta_o+\beta_1 \cdot \Delta Prec+\varepsilon$		
	R^2	β_1	*t* statistic	R^2	β_1	*t* statistic	R^2	β_1	*t* statistic	R^2	β_1	*t* statistic
Sahel	0.547	0.741	5.39[a]	0.475	0.665	4.56[a]	0.730	0.854	8.06[a]	0.647	0.758	6.50[a]
South Africa	0.782	0.885	9.28[a]	0.639	0.831	6.39[a]	0.693	0.832	7.36[a]	0.670	0.880	6.79[a]
South East Asia	0.149	0.386	2.05[b]	0.403	0.476	3.94[a]	0.167	0.408	2.19[b]	0.60	0.554	5.87[a]
Australia	0.371	0.609	3.76[a]	0.355	0.548	3.56[a]	0.546	0.739	5.38[a]	0.420	0.594	4.08[a]

Semi-arid tropic regions/pixels in our study refer to NDVI climatology values of 0.12 to 0.55 and 3 wettest months' precipitation values of less than 700 mm of rainfall.
[a]Statistically significant at the 0.001 level.
[b]Statistically significant at the 0.05 level.
β_o and β_1 are regression coefficients and ε is the stochastic error term.
LAI and Prec (precipitation) are all expressed as standardized anomalies. ΔLAI, ΔNDVI, and ΔPrec are first differences of the standardized anomalies.

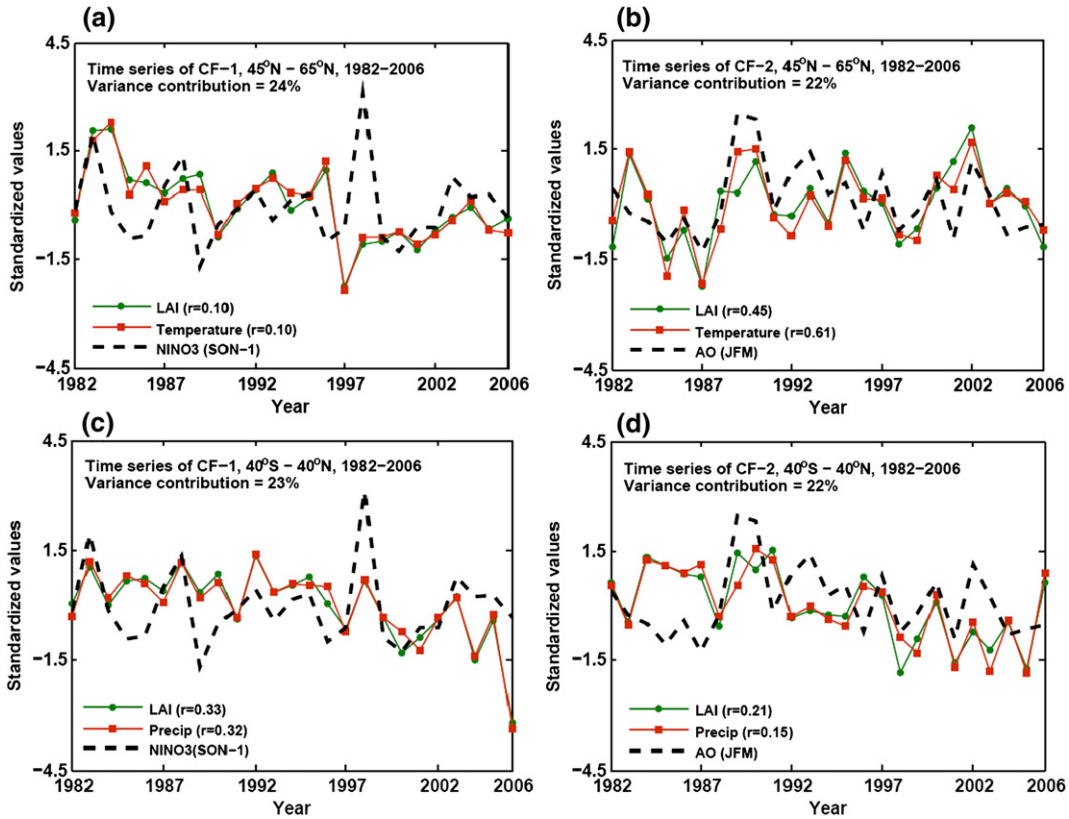

Fig. 9. Correlation between the standardized time series of the first canonical factor (CF-1, panels (a) and (c)) and second canonical factor (CF-2, panels (b) and (d)) with NINO3 and AO indices in the northern and tropical/sub-tropical regions.

semi-arid vegetation greenness and precipitation continues to be apparent. These results further add confidence in the LAI data set as we are not only able to reproduce previously reported results but also update them.

5. Validation with ground truth data

The validation of coarse resolution satellite products with ground measurements is a complicated task for several reasons — scaling

Table 4
Validation of AVHRR LAI with fine resolution LAI maps over different sites

Site name	Year (Month)	Area coverage	Biome	$\delta_{LAI,\ field}$	$\sigma_{LAI,\ field}$	$\delta_{LAI,\ AVHRR}$	$\sigma_{LAI,\ AVHRR}$
HARV[a]	2001 (July)	281*281 (25 m)	Deciduous broadleaf forests	5.370	0.852	5.260	0.561
KONZ[b]	2001 (July)	282*282 (25 m)	Grasslands	3.080	1.2584	2.584	1.325
TAPA[c]	2002 (Feb)	281*281 (25 m)	Evergreen broadleaf forests	4.140	1.530	6.110	0.987
NOBS[d]	2001 (Jul)	282*282 (25 m)	Needleleaf forests	2.890	1.621	1.960	0.423
Alpilles	2001 (Mar)	335*335 (30 m)	Grasses/cereal crops	1.030	0.890	0.890	0.265
Roukolahti	2001 (Jun)	500*500 (20 m)	Needleleaf forest	2.28	0.835	1.920	0.528
Canada Kejimikujik	2000 (Jul)	1000*1000 (30 m)	Needleleaf forests	3.530	1.495	4.001	1.318
Canada (Thompson)	2001 (Jul)	7680*7364 (30 m)	Needleleaf forests	1.885	0.858	1.750	0.419
Canada (Watson Lake)	2000 (Jul)	8930*8692 (30 m)	Needleleaf forests	2.390	1.080	1.402	0.532
Canada (Larose)	2003 (Aug)	800*800 (30 m)	Needleleaf forests	3.568	1.155	3.011	1.145

Mean (δ) and dispersion (σ) are measured with respect to valid retrievals over both field and satellite measured values.
Data reference for HARV, KONZ, NOBS and TAPA sites: BigFoot Measurements, Cohen et al. (2006).
Data reference for all the sites from Canada: Fernandes et al. (2005).
Data reference for Alpilles and Ruokolahti sites: Tan et al. (2005a,b) and Wang et al. (2004).
[a] HARV: Harvard Forest LTER, Massachusetts, USA.
[b] KONZ: Konza Prairie LTER, Kansas, USA.
[c] TAPA: Tapajos, Brazil.
[d] NOBS: BOREAS NSA, Canada.

of plot level measurements to sensor resolution, geo-location uncertainties, limited temporal and spatial sampling of ground data, field instrument calibration, sampling errors, etc. (Buermann et al., 2002; Huang et al., 2006; Tan et al., 2005a,b; Weiss et al., 2007; Yang et al., 2006a). In an indirect validation approach, such as inter-comparison of satellite products, the effects of co-registration and differences in spatial resolution can be minimized if the satellite products are compared at a coarser resolution (Tarnavsky et al., 2008; Weiss et al., 2007). In a direct validation such as with field measurements, spatial re-sampling is not always feasible because of inadequate sampling on the ground. The MODIS experience of LAI validation will be used to evaluate the AVHRR LAI data set. This work was performed within the purview of the Land Product Validation (LPV) LAI subgroup of the Committee Earth Observing Satellites' Working Group on Calibration and Validation (CEOS WGCV). Currently, a large number of US and international investigators participate in this activity by sharing field measured LAI/FPAR data as well as high-resolution maps though the ORNL DAAC Mercury system (Justice et al., 2000; Morisette et al., 2006). This large and growing data base provides the most up-to-date and comprehensive information needed for validation of LAI products. The scarcity of field LAI measurements during the 1980s and 90s represents a more challenging problem. Nevertheless, we attempted to utilize the available field data from multiple campaigns (Table A4, Appendix A) and high-resolution LAI maps (Table 4) to validate the AVHRR LAI product.

5.1. Validation with field/plot level observations

Most field measurements are typically several plot level samples within a small homogeneous region representing a certain vegetation type. An ideal field sampling of LAI must adequately represent its spatial distribution and cover the natural dynamic range within each major land cover type at the site (Yang et al., 2006b). On the other hand, the satellite retrievals cover an entire region of interest, but at a coarse scale. If the sampling in both cases is adequate, the LAI distributions from field measurements and satellite retrievals should ideally converge to the true intrinsic distribution of the vegetation class in a given region at a given time (Buermann et al., 2002). In this study, we selected sites with plot level measurements over homogeneous patches of a vegetation type. A pixel-by-pixel comparison between AVHRR LAI and reference field LAI values is not feasible for at least three reasons — first, the actual spatial location of the corresponding pixels in the two LAI maps may not match because of geo-location uncertainties and pixel-shift errors due to the point spread function (Tan et al., 2006); second, the AVHRR LAI algorithm generates a mean LAI value from all possible solutions corresponding to possible variation in input due to observation and model uncertainties (Knyazikhin et al., 1998). Therefore, the retrieved LAI value for a single 8 km pixel can differ from its measured counterpart, but the mean LAI of multiple pixels over a homogeneous patch may be valid (Wang et al., 2004); third, the spatial sampling for a particular field site can aggregate to an area which can be less than or equal to a single 8×8 km^2 AVHRR LAI pixel.

Mean LAI values from the 44 field measurements (28 sites) listed in Table A4 in Appendix A were used in this analysis. Monthly AVHRR LAI values from nearby pixels with the same vegetation type were averaged. This averaging window, centered on the field site, was typically about 2 by 2 or 4 by 4 pixels depending on the areal extent of the field site. The results of comparison for all the six major vegetation classes indicate that the AVHRR product underestimates field LAI by about 7% for LAI values greater than 1 (Fig. 10a). Additionally, we compared the temporal profile of LAI over three sites, Konza (grasslands), Mongu (savannas), and Harvard forest (broadleaf deciduous forest), for which there are more than one field value over the course of one or more years. Fig. 10b shows that the seasonal dynamics of *in situ* LAI over the Mongu site are well captured by the AVHRR LAI product, but are underestimates by 0.01–0.4 LAI. Similarly, the AVHRR LAI captures values of *in situ* LAI at the other two sites (Fig. 10a and c), but here the field samples are limited to a single measurement per year. For the Harvard forest site (Fig. 10c), the dip in the MODIS LAI values (July–Sep) is attributed to the retrieval anomalies over the broadleaf forests due to limited accuracy of atmospheric correction (Fig. 10c in Yang et al., 2006a). The number of high quality retrievals during the growing season is mostly restricted by aerosol contamination of the MODIS data (Fig. 9 in Yang et al., 2006a).

5.2. Validation with fine resolution LAI maps

Another approach to validation involves generation of fine resolution LAI maps from ground measurements and high-resolution satellite imagery such as ETM+, SPOT, ASTER, etc. using the so-called

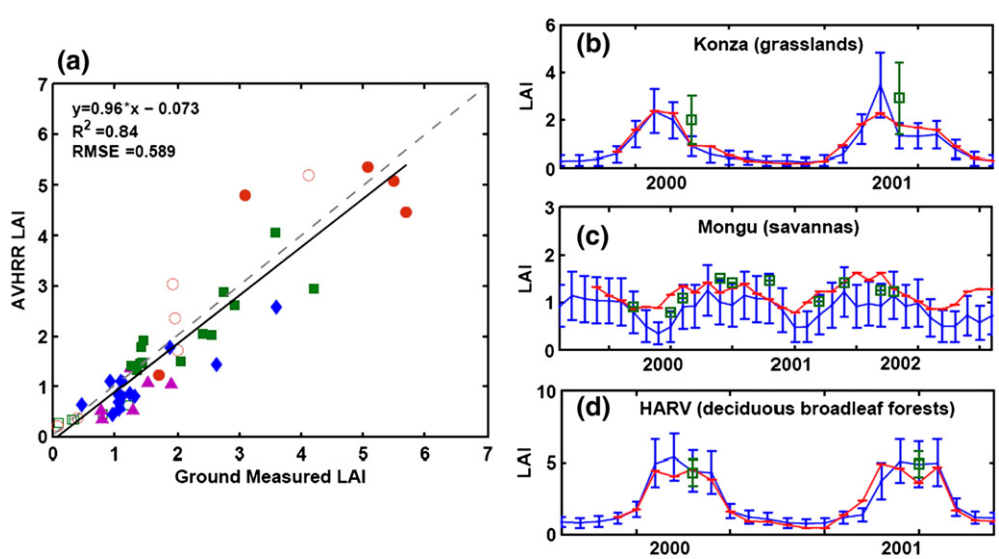

Fig. 10. Panel (a) shows a comparison of AVHRR LAI with field measurements for the six major vegetation classes. Altogether 44 field data values were used (Table A4 of Appendix A). The AVHRR LAI product is an underestimate by about 7%. Panels (b)–(d) show the temporal profile of AVHRR LAI (blue line), MODIS LAI (red line, MODIS starts from April 2000) and corresponding field values (green squares) for different vegetation classes. The vertical bars (blue and green) represent the standard deviation associated with the data. (For interpretation of the references to color in this figure legend, the reader is referred to the web version of this article.)

transfer function (Yang et al., 2006b). The transfer function could be empirical methods (Chen et al., 2002; Weiss et al., 2002), physical models (Tan et al., 2005a,b), or hybrid approaches (Weiss et al., 2002). Currently, several fine resolution maps are being disseminated via the ORNL DAAC Mercury system (Morisette et al., 2006). Maps from ten sites representing large homogeneous patches of distinct land cover types were used in this analysis (Table 4). The typical areal extent of these maps is between 50 km^2 to 100 km^2, except for the Canada Center for Remote Sensing sites (576 km^2–70,000 km^2). LAI distributions derived from blocks of 5 by 5 to 10 by 10 8 km AVHRR pixels were compared to LAI distributions from the fine resolution maps (Fig. 11). The AVHRR blocks were larger (30×30) for the Manitoba Black Spruce forest site at Thompson and the needleleaf forest site at Watson Lake.

Table 4 shows the mean values (δ) and corresponding dispersions (σ) for the distributions displayed in Fig. 11. In comparing the AVHRR LAI and fine resolution LAI distributions, there is a consistent underestimation at most sites possibly related to scale and land cover heterogeneity (Tian et al., 2002). The two distributions in general look different in terms of the dispersion from the mean value and this can be attributed to the differences in spatial scale and sampling strategies in generating the fine resolution maps. The difference in mean values from the distributions agree well for the Canadian sites, with $|\delta_{LAI,AVHRR}-\delta_{LAI,field}|$ of 0.47 LAI for the Kejimikujik conifer site and 0.13 LAI for the Manitoba Black Spruce forest at Thompson. For the Alpilles (grasses/cereal crops) and Ruokolahti (needleleaf forest) sites, the mean values of the distributions differ by about 0.14 and 0.36 LAI, respectively. As for the Konza, Harvard forest and Larose sites, the mean values differ by about 0.11 to 0.55 LAI. However, the AVHRR values for the broadleaf forest at Tapajos site in the Amazon underestimate the actual LAI values significantly, possibly due to poor NDVI quality as a result of persistent cloud cover and water vapor contamination. Significant underestimation in AVHRR values over the needleleaf forests is also observed for the NOBS site (0.93 LAI) and for the Watson lake site in Canada (0.98 LAI). The disagreement in the NOBS site is mainly due to landcover heterogeneity where the majority of the pixels are mapped as woody savannas and related classes (less than 60% tree cover) by BigFoot, but as evergreen needleleaf forests in the MODIS product (Cohen et al., 2006). The mean LAI retrievals from MODIS LAI over the NOBS site overestimate the BigFoot values by as much as 2 during peak growing season (Cohen et al., 2006), which is also reflected in the AVHRR retrievals. It is also to be noted that the Canadian product for the Manitoba black spruce forest at the NOBS site cannot be directly compared to the NOBS LAI maps from BigFoot due to differences in processing methods, plot scales and sampling schemes. Overall, amongst the ten sites, the AVHRR LAI values are in agreement to field observations at six of the select sites within an accuracy of 0.5 LAI.

6. Concluding remarks

In this second of two part series, the evaluation of a new global monthly AVHRR LAI data set for the period July 1981 to December 2006, derived from AVHRR NDVI is presented. The production of long term LAI data sets involves a host of inter-sensor related issues like differences in spatial resolution, spectral characteristics, uncertainties due to atmospheric effects and calibration, information content, etc. In the first paper, we introduced a physically based algorithm for the retrieval of LAI from AVHRR NDVI. The theoretical approach is based on the radiative transfer theory of spectral invariants and describes in detail the physical constraints as well as the conditions required to generate LAI fields of quality comparable to MODIS LAI products.

The theme of this paper is establishing the validity and accuracy of the derived LAI product. The evaluation of the data set is done both through direct comparisons to ground data and indirectly through inter-comparisons with similar data sets. This included comparisons with existing LAI products (MODIS and CYCLOPES LAI products for the 2000 to 2003 period of overlap) at a range of spatial scales, and correlations with key climate variables in areas where temperature and precipitation limit plant growth. There is an overall agreement between the AVHRR and MODIS data sets at scales ranging from global to regional to pixel. At the global scale, the AVHRR values explain 97.5% of the variability in the MODIS product and will be in error in their estimation by 0.18 LAI, on average. The regional and pixel-scale inter-comparison suggests an average error of less than 0.3 LAI. Comparison

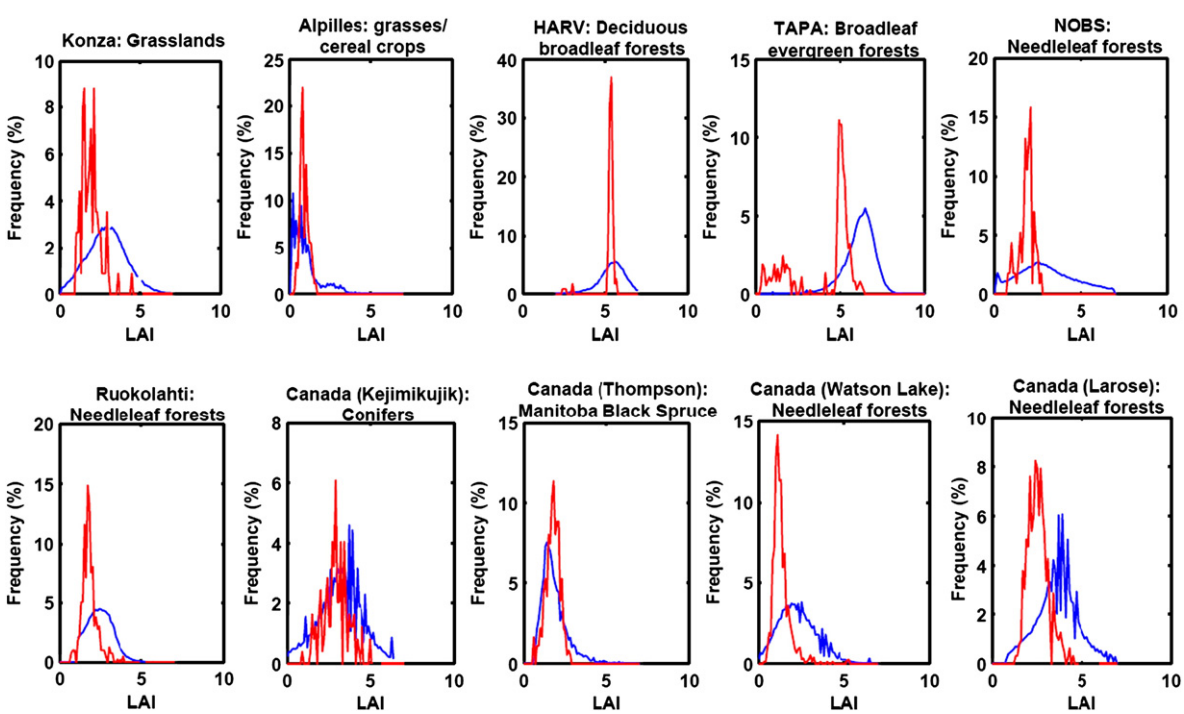

Fig. 11. Histograms from fine resolution LAI maps (blue color) and AVHRR LAI (red color) over different sites. Information about the sites is given in Table 4 together with values of accuracy and precision inferred from these distributions. (For interpretation of the references to color in this figure legend, the reader is referred to the web version of this article.)

with CYCLOPES LAI indicates satisfactory agreement in most of the biomes with RMSE values less than 0.5 LAI. The data set was also analyzed to reproduce well-documented spatio-temporal trends and inter-annual variations in vegetation activity in the northern latitudes, where temperature limits plant growth, and semi-arid areas, where precipitation limits plant growth. Additionally, to assess the mechanistic basis behind the observed correlations between LAI and temperature in the northern latitudes and LAI and precipitation in the semi-arid tropics, we used a multivariate data-reduction technique (canonical correlation analysis) to isolate well correlated modes of spatio-temporal variability between LAI and the climate variables. The isolated modes suggest El Niño-Southern Oscillation and Arctic Oscillation as key drivers of linked inter-annual variations in vegetation greenness and precipitation in the semi-arid regions and, vegetation greenness and surface temperature in the northern latitudes, respectively.

Finally, the derived LAI data were compared to field measurements and high-resolution LAI maps from a host of sites. The comparison with plot scale measurements over biome specific homogeneous patches indicates a 7% underestimation in the AVHRR LAI when all major vegetation types are considered. The error in mean values obtained from distributions of AVHRR LAI and high-resolution field LAI maps for different biomes is within 0.5 LAI for six out of the ten selected sites. These validation exercises though limited by the amount of field data, and thus less than comprehensive, nevertheless indicate comparability between the LAI product and field measurements. In summary, the inter-comparison with other short-term LAI data sets, evaluation of long term trends with known variations in climate variables, and validation with field measurements together build confidence in the utility of this new 26 year LAI record for long term vegetation monitoring and modeling studies.

Acknowledgements

This research was funded by NASA Earth Science Enterprise. We thank Dr. C. J. Tucker of NASA GSFC for making the GIMMS NDVI data available.

Appendix A. Ancillary tables

Table A1
Retrieval Index (RI), RMSE and mean single scattering albedo for different continents

LC	North America				Eurasia				Afro-Asia				South America			
	ω_{red}	ω_{NIR}	RI	Δ	ω_{red}	ω_{NIR}	RI	Δ	ω_{red}	ω_{NIR}	RI	Δ	ω_{red}	ω_{NIR}	RI	Δ
1	0.20	0.84	99	0.33	0.18	0.84	100	0.24	0.22	0.88	98	0.33	0.20	0.84	99	0.50
2	0.16	0.84	99	0.31	0.15	0.84	100	0.36	0.20	0.87	99	0.15	0.16	0.84	99	0.18
3	0.25	0.94	100	0.36	0.25	0.94	100	0.28	0.25	0.92	97	0.37	0.20	0.94	99	0.38
4	0.25	0.94	99	0.62	0.20	0.94	99	0.42	0.25	0.92	99	0.55	0.25	0.94	98	0.65
5	0.22	0.84	99	1.41	0.16	0.84	100	1.46	0.25	0.74	90	1.06	0.25	0.84	86	0.82
6	0.16	0.84	99	0.46	0.15	0.84	99	0.40	0.25	0.84	99	0.82	0.16	0.84	99	0.52
7	0.18	0.84	100	0.45	0.18	0.84	100	0.32	0.20	0.74	97	0.87	0.18	0.84	98	0.95
8	0.18	0.84	100	0.29	0.18	0.84	100	0.26	0.20	0.74	100	0.13	0.18	0.84	N/A	N/A

LC	North America	Eurasia	Afro-Asia	South America
	LC frequency (%)	LC frequency (%)	LC frequency (%)	LC frequency (%)
1	15.168	25.223	17.969	7.823
2	36.805	35.578	27.214	14.806
3	7.483	4.699	7.846	7.747
4	7.549	2.543	27.393	27.043
5	6.845	0.278	15.645	38.839
6	4.825	3.388	2.009	1.950
7	21.322	21.972	1.931	1.790
8	0.004	6.310	0.001	0

Here ω_{red} and ω_{NIR} are yearly mean values of single scattering albedo at red and NIR spectral band. "Δ" is the RMSE and "RI" refers to the retrieval index. LC in column one refers to the land cover type: 1 — grasses; 2 — shrubs; 3 — broadleaf crops; 4 — savannas; 5 — evergreen broadleaf forests; 6 — deciduous broadleaf forests; 7 — evergreen needleleaf forests; 8 — deciduous needleleaf forests. RI is expressed as percentage.

Table A2
Mean percentage difference and mean difference between global AVHRR and MODIS C5 LAI

LAI bins	% Mean difference	Mean difference	Number of pixels (%)
0–0.5	38.185	0.105	30.875
0.5–1.0	6.439	0.033	27.635
1.0–1.5	−10.223	−0.126	19.193
1.5–2.0	−5.459	−0.090	8.078
2.0–2.5	−1.280	−0.028	3.044
2.5–3.0	0.966	0.027	1.823
3.0–3.5	1.403	0.045	1.750
3.5–4.0	1.097	0.040	2.075
4.0–4.5	−1.755	−0.076	2.524
4.5–5.0	−5.971	−0.284	2.194
5.0–5.5	−9.283	−0.482	0.745
5.5–6.0	−12.747	−0.718	0.062
6.0–6.5	−20.505	−1.260	0.0003

Here "difference" refers to average annual LAI difference (AVHRR minus MODIS) for the year 2001.

Table A3
BELMANIP sites used for CYCLOPES LAI and AVHRR LAI inter-comparison

Site name (country)	Site ID	Lat	Lon	Biome type
ARM/CART Shilder (USA)	32	36.93°N	96.86°W	Grasses
Konza (USA)	36	39.08°N	96.57°W	Grasses
Larzac (France)	44	43.93°N	3.12°E	Grasses
Barrax (Spain)	35	39.07°N	2.10°W	Broadleaf crops
Alpilles (France)	43	43.80°N	4.74°E	Broadleaf crops
Plan-de Dieu (France)	45	44.20°N	4.95°E	Broadleaf crops
Fundulea (Romania)	47	44.40°N	26.58°E	Broadleaf crops
Tshane (Botswana)	7	24.00°S	21.83°E	Savannas
Okwa (Botswana)	8	22.40°S	21.71°E	Savannas
Mongu (Zambia)	11	15.44°S	23.25°E	Savannas
Burkina, Ghana (Burkina Faso)	385	10.86°N	3.07°W	Savannas
Kejimikujik (Canada)	48	44.35°N	65.19°W	Needleleaf forests
Thompson, Manitoba (Canada)	81	56.05°N	98.15°W	Needleleaf forests
NOBS-BOREAS NSA (Canada)	82	53.66°N	105.32°W	Needleleaf forests
Jarvselja (Estonia)	85	58.30°N	27.26°E	Needleleaf forests
Ruokolahti (Finland)	88	61.52°N	28.71°E	Needleleaf forests
Hirsinkanjas (Finland)	89	62.64°N	27.01°E	Needleleaf forests
Flakaliden (Sweden)	90	64.11°N	19.47°E	Needleleaf forests
Rovaniemi (Finland)	91	66.45°N	25.34°E	Needleleaf forests

Table A4
Summary of MODIS LAI field campaigns used for validation with AVHRR LAI

Site (country)	Lat/Lon	Biome type	Date	LAI
Bondville, Illinois (AGRO, USA)	40.007°N/88.292°W	Broadleaf crops	Aug 2000	3.60
Fundulea (Romania)	44.410°N/26.570°E	Broadleaf crops	(Mar, May) 2001	1.071, 1.878
			Jun 2002	1.309
			(May, Jun) 2003	1.063, 1.10
Barrax (Spain)	39.060°S/2.100°W	Broadleaf crops	Jul 2003	0.965
Alpilles (France)	43.810°N/4.750°E	Grasses/cereal crops	Mar 2001	0.928
			Jul 2002	1.054
Haouz (Morocco)	31.660°N/7.600°W	Shrubs	Mar 2003	1.20
Turco (Bolivia)	18.240°S/68.200°W	Shrubs	Apr 2003	0.10
Konza Prairie (USA)	39.080°N/96.570°W	Grasses	Jun 2000	1.96
Dahra (Senegal)	15.350°N/15.480°W	Grasses/savannas	Aug 2001	2.00
			Aug 2002	0.40
Pandamatenga (Botswana)	18.650°S/25.500°E	Savannas	Mar 2000	1.24
Maun (Botswana)	19.920°S/23.600°E	Savannas	Mar 2000	1.52
Mongu (Zambia)	15.440°S/23.253°E	Savannas	Apr 2000	1.90
			Sep 2000	0.80
Tessekre North	15.810°N/15.070°W	Shrubs	Aug 2002	0.35
Tessekre South (Senegal)		Shrubs	Aug 2002	0.30
Tshane (Botswana)	24.160°S/21.893°E	Savannas	Mar 2000	0.78
Okwa (Botswana)	22.400°S/21.713°E	Savannas	Mar 2000	1.28
Hirsikangas (Finland)	62.520°N/27.030°E	Needleleaf forests	Aug 2003	2.548
			Jun 2005	1.419
Ruokolahti (Finland)	61.320°N/28.430°E	Needleleaf forests	Jun 2000	2.06
Harvard Forest (HARV, USA)	42.530°N/72.173°W	Deciduous broadleaf forests	Jul 2000	5.08
			Jul 2001	5.50
Wisconsin (USA)	45.800°N/90.080°W	Deciduous broadleaf forests	May 2002	1.70
			Jul 2002	5.70
Concepcion (Chile)	37.467°S/73.470°E	Evergreen broadleaf forests	Jan 2003	3.096
Demmin (Germany)	53.892°N/13.207°E	Broadleaf crops	Jun 2004	2.632
Jarvselja (Estonia)	58.292°N/27.260°E	Needleleaf forests	Jul 2000	2.925
			Jun 2001	2.75
			Jun 2002	4.201
Laprida (Argentina)	36.990°S/60.552°W	Grasses	Nov 2001	4.124
			Oct 2002	1.923
Larose (Canada)	45.380°N/75.217°W	Needleleaf forests	Aug 2003	3.581
Nezer (France)	44.567°N/1.038°W	Needleleaf forests	Jul 2000	1.443
			Apr 2001	1.435
			Apr 2002	1.331
Plan-de-Dieu (France)	44.198°N/4.948°E	Broadleaf crops	Jul 2004	0.469
Rovaniemi (Finland)	66.455°N/25.351°E	Needleleaf forests	Jul 2004	1.248
			Jun 2005	1.401
Sud_Ouest (France)	43.506°N/1.237°E	Broadleaf crops	Jul 2002	1.228
Wankama (Niger)	13.644°N/2.635°E	Grasses	Jun 2005	0.081

The references regarding further description of site characteristics are provided in Table 1 of Yang et al., 2006a and Table 4 of this paper.
Detailed methodologies and documentation of field campaigns can be obtained from http://mercury.ornl.gov/ornldaac/ and http://lpvs.gsfc.nasa.gov/lai_intercomp.php.

References

Angert, A., Biraud, S., Bonfils, C., Henning, C. C., Buermann, W., Pinzon, J., et al. (2005). Drier summers cancel out the CO_2 uptake enhancement induced by warmer springs. *Proceedings of the National Academy of Sciences USA*, *102*, 10823–10827.

Barber, V. A., Juday, G. P., & Finney, B. P. (2000). Reduced growth of Alaskan white spruce in the twentieth century from temperature-induced drought stress. *Nature*, *405*, 668–673.

Baret, F., Morissette, J., Fernandes, R., Champeaux, J. L., Myneni, R. B., Chen, J., et al. (2006). Evaluation of the representativeness of networks of sites for the global validation and inter-comparison of land biophysical products. Proposition of the CEOS-BELMANIP. *IEEE Transactions on Geoscience and Remote Sensing*, *42*(7), 1794–1803.

Baret, F., Hagolle, O., Geiger, B., Bicheron, P., Miras, B., Huc, M., et al. (2007). LAI, fAPAR, and fCover CYCLOPES global products derived from VEGETATION Part 1: Principles of the algorithm. *Remote Sensing of Environment*, *110*, 275–286.

Barnett, T. P., & Preisendorfer, R. (1987). Origins and levels of monthly and seasonal forecast skill for United States surface air temperatures determined by canonical correlation analysis. *Monthly Weather Review*, *115*, 1825–1850.

Bjornsson, H., & Venegas, S.A. (1997). A manual for EOF and SVD analysis of climate data. McGill University, CCGCR Report No. 97-1, Montreal, Quebec, pp. 52.

Brown, M. E., Pinzon, J. E., Morisette, J. T., Didan, K., & Tucker, C. J. (2006). Evaluation of the consistency of long term NDVI time series derived from AVHRR, SPOT-Vegetation, SeaWIFS, MODIS, and Landsat ETM+. *IEEE Transactions Geosciences and Remote Sensing*, *44*(7), 1787–1793.

Buermann, W., Wang, Y., Dong, J., Zhou, L., Zeng, X., Dickinson, R. E., et al. (2002). Analysis of a multiyear global vegetation leaf area index data set. *Journal of Geophysical Research*, *107*, 1–15.

Buermann, W., Anderson, B., Tucker, C. J., Dickinson, R. E., Lucht, W., Potter, C. S., et al. (2003). Interannual covariability in northern hemisphere air temperatures and greenness associated with El Niño-Southern oscillation and the Arctic oscillation. *Journal of Geophysical Research*, *108*, 1–16.

Bunn, A. G., & Goetz, S. J. (2006). Trends in satellite-observed circumpolar photosynthetic activity from 1982 to 2003: The influence of seasonality, cover type, and vegetation density. *Earth Interactions*, *10*(12), 1–19.

Chen, J. M., Pavlic, G., Brown, L., Cihlar, J., Leblanc, S. G., White, H. P., et al. (2002). Derivation and validation of Canada-wide coarse resolution leaf area index maps using high-resolution satellite imagery and ground measurements. *Remote Sensing of Environment*, *80*, 165–184.

Cohen, W. B., Maiersperger, T. K., Turner, D. P., Ritts, W. D., Pflugmacher, D., Kennedy, R. E., et al. (2006). MODIS land cover and LAI collection 4 product quality across nine sites in the western hemisphere. *IEEE Transactions on Geoscience and Remote Sensing*, *44*(7), 1843–1857.

Dai, A., & Wigley, T. M. L. (2000). Global patterns of ENSO-induced precipitation. *Geophysical Research Letter*, *27*, 1283–1286.

Dai, A., Fung, I. Y., & Del Genio, A. D. (1997). Surface observed global land precipitation variations during 1900–88. *Journal of Climate*, *10*, 2943–2962.

Demarty, J., Chevallier, F., Friend, A. D., Viovy, N., Piao, S., & Ciais, P. (2007). Assimilation of global MODIS leaf area index retrievals within a terrestrial biosphere model. *Geophysical Research Letters*, *34*, L15402. doi:10.1029/2007GL030014.

Dickinson, R. E., Hendersen-Sellers, A., Kennedy, P. J., & Wilson, M. F. (1986). Biosphere–Atmosphere Transfer Scheme (BATS) for the NCAR CCM, *NCAR Res.*, Boulder, CO, NCAR/TN-275-STR.

Fernandes, R. A., Abduelgasim, A., Sylvain, L., Khurshid, S. K., & Butson, C. (2005). Leaf area index maps at 30-m resolution, selected sites, Canada. Data set. Available online [http://daac.ornl.gov/] from Oak Ridge National Laboratory Distributed Active Archive Center, Oak Ridge, Tennesse, U.S.A.

Ganguly, S., Schull, M. A., Samanta, A., Shabanov, N. V., Milesi, C., Nemani, R. R., et al. (in press). Generating vegetation leaf area index earth system data record from multiple sensors. Part 1: Theory. *Remote Sensing of Environment*. doi:10.1016/j.rse.2008.07.014.

GCOS, 2006 GCOS, Systematic observation requirements for satellite-based products for climate. WMO/TD No. 1338. September 2006 (2006) 103 pp. (available at http://www.wmo.ch/web/gcos/gcoshome.html).

Gobron, N., Pinty, B., Verstraete, M., & Govaerts, Y. (1999). MERIS Global Vegetation Index (MGVI): Description and preliminary application. *International Journal of Remote Sensing*, *20*, 1917–1927.

Goetz, S. J., Bunn, A. G., Fiske, G. J., & Houghton, R. A. (2005). Satellite-observed photosynthetic trends across boreal North America associated with climate and fire disturbance. *Proceedings of the National Academy of Sciences USA*, *102*, 13521–13525.

Hansen, J., Ruedy, R., Glascoe, J., & Sato, M. (1999). GISS analysis of surface temperature change. *Journal of Geophysical Research*, *104*, 30997–31022.

Herrmann, S. M., Anyamba, A., & Tucker, C. J. (2005). Recent trends in vegetation dynamics in the African Sahel and their relationship to climate. *Global Environmental Change*, *15*, 394–404.

Hickler, T., Eklundh, L., Seaquist, J. W., Smith, B., Ardö, J., Olsson, L., et al. (2005). Precipitation controls Sahel greening trend. *Geophysical Research Letters*, *32*, 1–4.

Holben, B. (1986). Characteristics of maximum-value composite images from temporal AVHRR data. *International Journal of Remote Sensing*, *7*, 1417–1434.

Huang, D., Yang, W., Tan, B., Rautiainen, M., Zhang, P., Hu, J., et al. (2006). The importance of measurement errors for deriving accurate reference leaf area index maps for validation of moderate-resolution satellite LAI products. *IEEE Transactions on Geoscience and Remote Sensing*, *44*(7), 1866–1871.

Huffman, G. J., Adler, R. F., Bolvin, D. T., Gu, G., Nelkin, E. J., Bowman, K. P., et al. (2007). The TRMM multi-satellite precipitation analysis: Quasi-global, multi-year, combined-sensor precipitation estimates at fine scale. *Journal of Hydrometeorology*, *8*(1), 38–55.

Justice, C., Belward, A., Morisette, J., Lewis, P., Privette, J., & Baret, F. (2000). Developments in the 'validation' of satellite sensor products for the study of the land surface. *International Journal of Remote Sensing*, *21*, 3383–3390.

Knyazikhin, Y., Martonchik, J. V., Myneni, R. B., Diner, D. J., & Running, S. W. (1998). Synergistic algorithm for estimating vegetation canopy leaf area index and fraction of absorbed photosynthetically active radiation from MODIS and MISR data. *Journal of Geophysical Research*, *103*, 32257–32274.

Lapenis, A., Shvidenko, A., Shepaschenko, D., Nilsson, S., & Aiyyer, A. (2005). Acclimation of Russian forests to recent changes in climate. *Global Change Biology*, *11*, 2090–2102.

Masson, V., Champeaux, J. L., Chauvin, F., Meriguer, C., & Lacaze, R. (2003). A global database of land surface parameters at 1 km resolution in meteorological and climate models. *Journal of Climate*, *16*, 1261–1282.

Mitchell, T. D., & Jones, P. D. (2005). An improved method of constructing a database of monthly climate observations and associated high-resolution grids. *International Journal of Climatology*, *25*(6), 693–712.

Miura, T., Huete, A. R., & Yoshioka, H. (2000). Evaluation of sensor calibration uncertainties on vegetation indices for MODIS. *IEEE Transactions on Geoscience and Remote Sensing*, *38*(3), 1399–1409.

Morisette, J. T., Baret, F., Privette, J. L., Myneni, R. B., Nickeson, J. E., Garrigues, S., et al. (2006). Validation of global moderate resolution LAI products: A framework proposed within the CEOS land product validation subgroup. *IEEE Transactions in Geoscience and Remote Sensing*, *44*, 1804–1817.

Myneni, R. B., Keeling, C. D., Tucker, C. J., Asrar, G., & Nemani, R. R. (1997). Increased plant growth in the northern high latitudes from 1981–1991. *Nature*, *386*, 698–701.

Nemani, R. R., Keeling, C. D., Hashimoto, H., Jolly, W., Piper, S. C., Tucker, C. J., et al. (2003). Climate-driven increases in global terrestrial net primary production from 1981 to 1999. *Science*, *300*, 1560–1563.

North, G. R., Bell, T. L., Cahalan, R. F., & Moeng, F. J. (1992). Sampling errors in the estimation of empirical orthogonal functions. *Monthly Weather Review*, *110*, 699–706.

Pinzon, J. E., Brown, M. E., & Tucker, C. J. (2005). Satellite time series correction of orbital drift artifacts using empirical mode decomposition. In N. Huang (Ed.), *Hilbert–Huang transform: Introduction and applications* chapter 10, part II. applications.

Plummer, S., Arino, O., Simon, W., & Steffen, W. (2006). Establishing an Earth observation product service for the terrestrial carbon community: The GLOBCARBON initiative. *Mitigation and Adaptation Strategies for Global Change*, *11*, 97–111.

Prince, S. D., Wessels, K. J., Tucker, C. J., & Nicholson, S. E. (2007). Desertification in the Sahel: A reinterpretation of a reinterpretation. *Global Change Biology*, *13*, 1308–1313.

Ropelewski, C. F., & Halpert, M. S. (1987). Global and regional scale precipitation pattern associated with El Nino/Southern Oscillation. *Monthly Weather Review*, *115*, 1606–1626.

Seaquist, J. W., Olsson, L., Ardo, J., & Eklundh, L. (2006). Broad-scale increase in NPP quantified for the African Sahel, 1982–1999. *International Journal of Remote Sensing*, *27*, 5115–5122.

Sellers, P. J., Randall, D. A., Collatz, G. J., Berry, J. A., Field, C. B., Dazlich, D. A., et al. (1996). A revised land surface parameterization (SiB2) for atmosphere GCMs. Part II: The generation of global fields of terrestrial biophysical parameters from satellite data. *Journal of Climate*, *9*, 706–737.

Shabanov, N. V., Huang, D., Yang, W., Tan, B., Knyazikhin, Y., Myneni, R. B., et al. (2005). Optimization of the MODIS LAI and FPAR algorithm performance over broadleaf forests. *IEEE Transactions in Geoscience and Remote Sensing*, *43*, 1855–1865.

Slayback, D. A., Pinzon, J. E., Los, S. O., & Tucker, C. J. (2003). Northern hemisphere photosynthetic trends 1982–1999. *Global Change Biology*, *9*, 1–15.

Soja, A. J., Tchebakova, N. M., French, N. H. F., Flannigan, M. D., Shugart, H. H., Stocks, B. J., et al. (2007). Climate-induced boreal forest change: Predictions versus current observations. *Global and Planetary Change*, *56*, 274–296.

Tan, B., Hu, J., Zhang, P., Huang, D., Shabanov, N. V., Weiss, M., et al. (2005). Validation of MODIS LAI product in croplands of Alpilles, France. *Journal of Geophysical Research*, *110*, 1–15.

Tan, B., Hu, J., Huang, D., Yang, W., Zhang, P., Shabanov, N. V., et al. (2005). Assessment of the broadleaf crops leaf area index product from the Terra MODIS instrument. *Agricultural and Forest Meteorology*, *135*, 124–134.

Tan, B., Woodcock, C. E., Hu, J., Zhang, P., Ozdogan, M., Huang, D., et al. (2006). The impact of gridding artifacts on the local spatial properties of MODIS data: Implications for validation, compositing, and band-to-band registration across resolutions. *Remote Sensing of Environment*, *105*, 98–114.

Tape, K., Sturm, M., & Racine, C. (2006). The evidence for shrub expansion in northern Alaska and the pan-Arctic. *Global Change Biology*, *12*, 686–702.

Tarnavsky, E. V., Garrigues, S., & Brown, M. E. (2008). Multiscale geostatistical analysis of AVHRR, SPOT-VGT, and MODIS global NDVI products. *Remote Sensing of Environment*, *112*, 535–549.

Thompson, D. W. J., & Wallace, J. M. (1998). The Arctic oscillation signature in the wintertime geopotential height and temperature fields. *Geophysical Research Letters*, *25*, 1297–1300.

Tian, Y., Wang, Y., Zhang, Y., Knyazikhin, Y., Bogaert, J., & Myneni, R. B. (2002). Radiative transfer based scaling of LAI/FPAR retrievals from reflectance data of different resolutions. *Remote Sensing of Environment*, *84*, 143–159.

Tian, Y., Dickinson, R. E., Zhou, L., Zeng, X., Dai, Y., Myneni, R. B., et al. (2004). Comparison of seasonal and spatial variations of LAI/FPAR from MODIS and common land model. *Journal of Geophysical Research*, *109*, D01103. doi:10.1029/2003JD003777.

Tucker, C. J., Pinzon, J. E., Brown, M. E., Slayback, D. A., Pak, E. W., Mahoney, R., et al. (2005). An Extended AVHRR 8-km NDVI data set compatible with MODIS and SPOT Vegetation NDVI Data. *International Journal of Remote Sensing*, *26*(20), 4485–5598.

Van Leeuwen, W. J. D., Orr, B. J., Marsh, S. E., & Herrmann, S. M. (2006). Multi-sensor NDVI data continuity: Uncertainties and implications for vegetation monitoring applications. *Remote Sensing of Environment*, *100*, 67–81.

Wang, Y., Tian, Y., Zhang, Y., El-Saleous, N., Knyazikhin, Y., Vermote, E., et al. (2001). Investigation of product accuracy as a function of input and model uncertainties: Case study with SeaWiFS and MODIS LAI/FPAR algorithm. *Remote Sensing of Environment*, *78*, 296–311.

Wang, Y., Woodcock, C. E., Buermann, W., Stenberg, P., Voipio, P., Smolander, H., et al. (2004). Evaluation of the MODIS LAI algorithm at a coniferous forest site in Finland. *Remote Sensing of Environment*, *91*, 114–127.

Weiss, M., Baret, F., Leroy, M., Hautecoeur, O., Bacour, C., Prevot, L., et al. (2002). Validation of neural net techniques to estimate canopy biophysical variables from remote sensing data. *Agronomie*, *22*, 547–553.

Weiss, M., Baret, F., Garrigues, S., & Lacaze, R. (2007). LAI and fAPAR CYCLOPES global products derived from VEGETATION. Part 2: Validation and comparison with MODIS collection 4 products. *Remote Sensing of Environment*, *110*, 317–333.

Wilmking, M., Juday, G. P., Barber, V. A., & Zald, H. S. J. (2004). Recent climate warming forces contrasting growth responses of white spruce at treeline in Alaska through temperature thresholds. *Global Change Biology*, *10*, 1724–1736.

Yang, W., Shabanov, N. V., Huang, D., Wang, W., Dickinson, R. E., Nemani, R. R., et al. (2006). Analysis of leaf area index product from combination of MODIS and Aqua data. *Remote Sensing of Environment*, *104*, 297–312.

Yang, W., Tan, B., Huang, D., Rautiainen, M., Shabanov, N. V., Wang, Y., et al. (2006). MODIS leaf area index products: From validation to algorithm improvement. *IEEE Transactions on Geoscience and Remote Sensing*, *44*, 1885–1898.

Zhou, L., Tucker, C. J., Kaufmann, R. K., Slayback, D., Shabanov, N. V., & Myneni, R. B. (2001). Variations in northern vegetation activity inferred from satellite data of vegetation index during 1981 to 1999. *Journal of Geophysical Research*, *106*, 20069–20083.

WWW Sites

WWW1: MODIS land validation approach. http://landval.gsfc.nasa.gov/ProductStatus.php?ProductID=MOD15

WWW2: MODIS LAI readme manual. ftp://primavera.bu.edu/pub/datasets/MODIS/readme.pdf

WWW3: Monthly Atmospheric and SST Indices, NOAA/NWS/NCEP Climate Prediction Center. http://www.cpc.ncep.noaa.gov/data/indices/wksst.for

WWW4: Climate Diagnostics Bulletin, NOAA/NWS/NCEP Climate Prediction Center, December, 2007. http://www.cpc.ncep.noaa.gov/products/CDB/Tropics/figt5.shtml